STUDIES ON DIELECTRIC PROPERTIES OF CALCIUM COPPER TITANATE AT DIFFERENT SINTERING CONDITIONS

A dissertation submitted in the partial fulfillment of requirement for the award of the degree of

Master of Technology
in
MATERIALS SCIENCE AND METALLURGY

Submitted by

RAVINDRA KUMAR

Roll No. : 600802024

Carried out at

Electronic Material Division
Advance Ceramic Section
National Physical Laboratory
New Delhi-110012

School of Physics and Materials Science
Thapar University
Patiala (Punjab)-147004

June 2010

CERTIFICATE

This is to certify that the project work entitled "*Studies on dielectric properties of calcium copper titanate at different sintering conditions*" is an authentic record of the work carried out by RAVINDRA KUMAR (600802024) in partial fulfillment of the requirements for the award of the degree of Master of Technology (Material Science and Metallurgy) of Thapar University, Patiala, under my guidance and supervision.

Supervisors

Dr. Kulvir Singh

Associate Professor
School of Physics and Material Science
Thapar University
Patiala-147004

Dr. T.D.Senguttuvan

Scientist "E1"
Advance Ceramic & Devices Section
National Physical Laboratory
NewDelhi-110012

Countersigned by:

Dr.O.P.Pandey

Prof & Head
School of Physics and Material Science
Thapar University
Patiala-147004

Dr. R.K. Sharma 18.8.10

Dean, Academic Affair
Thapar University
Patiala-147004

DECLARATION

I hereby declare that this project report entitled *"Studies on dielectric properties of calcium copper titanate at different sintering conditions"* is an authentic report of the work done by me under the guidance of Dr. T. D. Senguttuvan, Scientist "E1", National Physical Laboratory, New Delhi-110012 and Dr. Kulvir Singh. It is an original and independent work done by me.

Ravindra Kumar

(Ravindra Kumar)
Roll No. 600802024
Thapar University
Patiala

DEDICATION

I would like to dedicate this dissertation to my parents, Shri Ram Baksh Nimesh and Smt. Krishna Devi, my brother Man Singh, my sister Jyoti, my Jija Ji Harish Chand and my sister Rajbala for their inspiration, devotion, faith and support throughout this process.

ACKNOWLEDGEMENT

This thesis work is the final examination toward getting my master degree in Materials and Metallurgical Engineering at Thapar University, Patiala. The work has been carried out with the huge blessing of **God**.

I would like to express my deepest gratitude to **Dr. T.D.Senguttuvan** for providing me an opportunity to work in for Advance Ceramic lab, NPL. His astonishing language skills and his clear vision of scientific content help me in tremendous manner. His excellent ideas and precious comments have inspired me and taught me a great deal, his strong confidence and farsighted outlook gave me confidence and enhanced my pleasure in the work. Without his genuine concern and unreserved support, I could not have finished my thesis work successfully.

I also would like to thank my supervisor **Dr. Kulvir Singh, Associate Professor** who has given me treasured ideas and valuable advice. Moreover, I am indebted to **Prof. O.P.Pandey**, Head, School of Physics and Material Science, Thapar University, Patiala for his support. Special acknowledgements are given to **Director NPL,** for permitting and providing the facilities necessary for carrying out thesis work at NPL.

I am deeply indebted to my teachers, Dr. K.K.Raina, Dr. N.K.Verma, Dr. Sunil Kumar, Dr. Manoj Kumar, Dr. D.P.Singh, Dr. Puneet Sharma, Dr. Loveleen Brar and Dr. S.D.Tiwari. Their ideals and concepts have had a remarkable influence on my understanding in the field of Material Science and Engineering.

I am very thankful to **Dr. Rajeev Chopra,** Scientist 'F' Head, Human Resources Development (HRD), NPL, who has readily granted me the permission and providing an opportunity to work at this premier laboratory, NPL.

I would like to give my special thanks to Mr. Ranjeet Kumar, Mrs Gurbinder chaudhary, Miss Monika Mishra, Mr. Prabal Pratap Singh, Mr. Vaibhav Koutu, for their kind support in my work. Mr. Ranjeet Kumar helped me in all possible ways. Their timely discussions are very much appreciable.

I also would like to thanks my naughty friends Mr. Anil Kumar, Mr. N.P.Mishra, Mr. Mukesh Kumar.

Lastly I would like to thanks Mr. Raju for their help in arranging laboratory materials during experiments.

Ravindra Kumar

Ravindra Kumar

ABSTRACT

$CaCu_3Ti_4O_{12}$ (CCTO) electroceramic was prepared by a solid state reaction technique from $CaCO_3$, CuO and TiO_2 powders. Processing involved the raw material and their and milling, calcination, pellet forming and sintering processes. The calcination of CCTO was carried out at 1000°C for 24 hours in glowber furnace. The formation of CCTO is confirmed by XRD. Samples were sintered at different temperature in order to improve phase structure,density, homogeneity, morphology and dielectric properties of CCTO ceramics. The morphology and size of the grains of the pellets were observed using scanning electron microscopy (SEM). SEM images show that the grain size of sintered samples is increasing with increase of sintering temperature. The dielectric properties of the samples were analyzed in the wide range of frequency (10^2 - 10^7 Hz). Dielectric studies shows that dielectric constant is increasing with increasing sintering temperature and holding time while tanδ remains almost same after 2 h heat treated sample and decreased for 10 h. It is found that on increasing grain size which is obtained by rising the sintering temperature, the dielectric properties are enhanced.

List of abbreviation and terms

CCTO	Calcium Copper Titanium oxide
IBLC	Internal barrier layer capacitance
Tm	Melting point
SEM	Scanning electron microscopy
XRD	X ray Diffraction
Cgb	Grain boundary capacitance
Cb	Bulk capacitance
CIP	Cold isostatic pressing
PVA	Poly vinyl alcohol
Eps'	Real part of Dielectric constant
Eps"	Imaginary part of Dielectric constant

LIST OF FIGURES AND TABLES

Tables

INDEX

CONTENTS

CHAPTER 1

INTRODUCTION

Scientists in all over the world are putting efforts to develop a material that may lead to significant advances in the miniaturisation of electronics. These materials can be used as a high performance capacitors and offer insight into how charges behave on the nano scale (order of billionths of a meter). However, great challenge in microelectronic field is to decrease the size of passive components and particularly the capacitors one. For these reasons there has been a considerable interest in the study of the giant dielectric permittivity of the cubic ABO_3 perovskite type in the last decade. The $CaCu_3Ti_4O_{12}$ compound (CCTO) has recently attracted much interest due to its extraordinarily high static dielectric constant up to 10^5 which is practically frequency independent up to10^6 Hz and possesses good temperature stability over a temperature range between -173°C and 127°C. Extremely high dielectric constant does not vary significantly in the frequency range from 20 Hz to 1 MHz at room temperature. This extremely high dielectric constant is usually associated to ferroelectric or relaxor materials. However CCTO structure remains centrosymmetric at all temperatures with no phase transitions. The unit cell of this titanate was identified in 1979 as a body centred cubic perovskite like structure with Im3 space group and a lattice parameter of 7.391A°. The TiO_6 octahedra are tilted resulting in the doubling of the perovskite like lattice parameter and involving a square planar arrangement of the oxygen around the Cu^{2+} cations.

Subramanian et al. [1] have first reported the high dielectric constant at 1 kHz in $ACu_3Ti_4O_{12}$ and $ACu_3Ti_3FeO_{12}$ phases (A=trivalent rare earth or Bi). Values of permittivity, *ε'*, higher than 10000, have been reported for ceramics and for single crystals. The real part of the permittivity has been even increased from 10^4 to $3x10^5$ as a result of grain growth. Studies of CCTO thin

films prepared by pulsed laser deposition confirm that large mean grain size may be responsible for the high dielectric constant. Moreover the high dielectric constant does not depend on the temperature which makes it even more attractive for technological applications even if the dielectric losses which are in most cases very high have also to be taken into account.

1.1. Structure of $CaCu_3Ti_4O_{12}$ (CCTO):

The extended unit cell structure of CCTO is shown in Fig1.1. Following the first details on the $ACu_3Ti_4O_{12}$ family by a group of French researchers in 1967, Bochu et al [2] reported the detailed and more precise structural analysis of these compounds in 1979. Based on their study CCTO possesses a distorted cubic perovskite (ABO_3) structure with the space group Im3 and a lattice parameter of 7.391A°. Here the Ca^{2+} ions occupy the corners and the center of the unit cell while Cu^{2+} ions are located on the centers of cell edges and planes. The Ti^{4+} ions are surrounded by 6 oxygen ions forming TiO_6 octahedra which are tilted inward in order to make a square planar arrangement for the nearby Cu^{2+} ions. Structures with Cu^{2+} in a square planar configuration are common in compounds with a d^9 electron configuration. This results from d orbital splitting such that the dx^2-y^2 state shifts to a higher energy state occupied by a single electron while the dz^2 state takes on a lower energy state with a pair of electrons. This phenomenon is called the Jahn Teller effect or 6 distortions is usually achieved by increasing the bond length along the z axis which consequently causes a reduction in the electron pair repulsion [3] and a tilt of the TiO_6 octahedra in CCTO. Subramanian et al.[4] mentioned that the enhanced polarizability and the dielectric constant in CCTO could be due to the tension of the Ti-O bonds and that the extreme tilt of the TiO_6 octahedra prevents the formation of the ferroelectric state. Although the high dielectric constant in CCTO can be explained from the structural point of view there have been many reports that strongly indicate that the other mechanisms are possible.

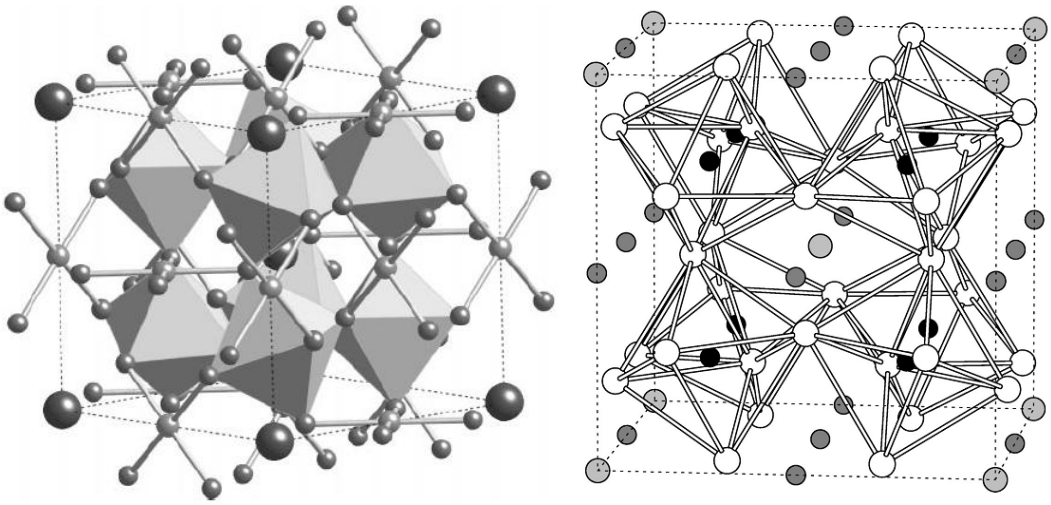

Fig. 1.1 Three dimensional unit cell structure of CCTO [Ca is the largest atom at the corners and the center of a unit cell; Cu atom is located in the center of edges and facial planes in a unit cell; Ti atom is hidden inside of each octahedron, forming TiO_6; four O atoms are bonded to a single Cu atom – CuO_4 square planar structure][5].

1.2 Origin of the high dielectric constant in CCTO:

Many theories have been proposed to explain the origin of high dielectric constant of CCTO. Ramirez et al. [6] and Homes et al. [7] have tried to explain it from the intrinsic point of view. Ramirez et al [6] reported that below 100K the dielectric constant drops abruptly from around 12000 to as low as 100 in addition to the fact that CCTO holds a large dielectric constant that barely varies in the temperature range from 100 K to 400 K as shown in Fig. 1.2. The reported dielectric loss or tanδ is less than 0.1 when the temperature is higher than 150 K and a large peak occurs at around 100K. Frequency dependence is also shown from 100 K to 300 K in a wide frequency range between 10^2 Hz to 10^6 Hz for both dielectric constant and loss. With the increasing frequency the dielectric constant decreases in the entire temperature range and the dielectric loss peak shifts to higher temperature with small increase in the maximum value of the peak. Based upon this study they suggested that the anomalous dielectric responses in CCTO might be linked to a Debye like relaxation behavior. Homes et al. [7] suggested the relaxor like

slowing down of the dipolar fluctuations in nano sized domains as the possible mechanism for the unusually high dielectric constant in CCTO.

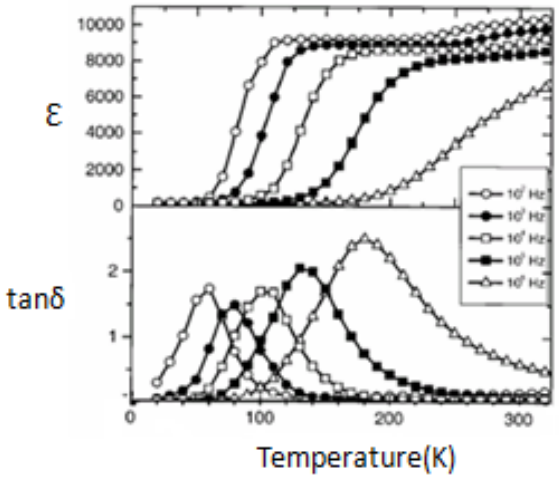

Fig. 1.2 Temperature dependence of ε' and tan δ at 10^2, 10^3, 10^4, $10^5$and 10^6 Hz[6].

This theory states that the dielectric behavior of CCTO does not come from its intrinsic character but from some heterogeneity of its ceramic structure. During the sintering step of any $ATiO_3$ based samples (where A= Ca, Sr and Ba), they lose small amounts of oxygen and become conductive. Correspondingly certain reoxidation creates insulating layers on the surface and along the internal boundaries of individual grains which is considered to be the origin of the giant dielectric constant of CCTO. This creates an electrically inhomogeneous structure that is characterized by the spatially varying permittivity at the micro or nano scale. The most well known examples of this barrier layer capacitor are barium and strontium titanates ($BaTiO_3$, $SrTiO_3$). In order to verify the enhanced dielectric constant in the barrier layer materials consisting of semiconducting grains and insulating grain boundaries the simple brick wall model was suggested [8].

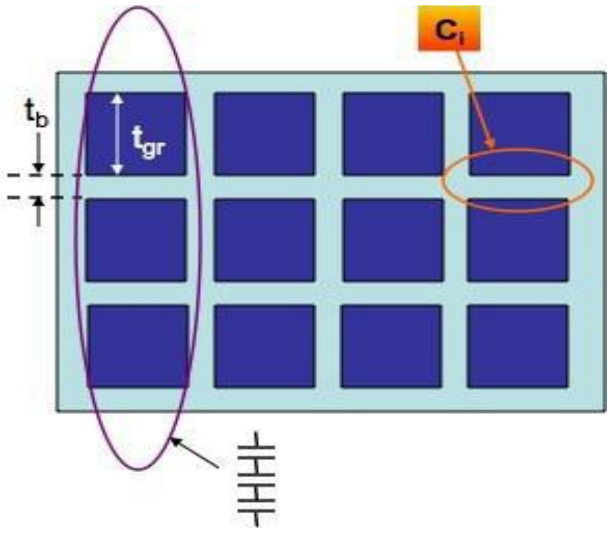

Fig. 1.3 Brick wall model for a barrier layer capacitor[9].

Assuming the simplified microstructure (shown in Figure. 1.3) where the grain boundary thickness is much smaller than the grain size the capacitance of a single element can be expressed by:

$$Ci = \frac{\varepsilon_0 \varepsilon_r t_{gr}^{\ 2}}{t_B} \qquad \ldots(1.1)$$

Also if a column of elements is connected in series i.e. (1/C = 1/C1 + 1/C2 + …..) Eq. (1.1) becomes

$$\frac{Ci}{no.\,of\ element} = \frac{\varepsilon_o \varepsilon_r t_{gr}^{\ 2} \,/\, t_B}{t \,/\, t_{gr}} \qquad \ldots(1.2)$$

By calculating the capacitance per unit area (C/A), the effective dielectric constant of the barrier layer material is

$$\varepsilon_{eff} = \frac{\varepsilon_0 t_{gr}}{t_g} \qquad \ldots(1.3)$$

The first evidence of this barrier layer capacitor model for CCTO was reported by Sinclair et al. [10] by using the impedance spectroscopy. An ideal equivalent circuit that includes two parallel resistance capacitor (RC) elements connected in series shown in Fig. 1.4 (a). The impedance data represented as the reactance (Z'') in the y axis and the resistance (Z') in the x axis indicate two semi circles representing both the grain and grain boundary response. Here the resistances are obtained from the intercepts on the x axis while the capacitances can be calculated by using the given equation (1.4):

$$\omega_{max}\, RC = 1 \qquad \ldots(1.4)$$

where, ω_{max} is the frequency at the maximum Z" of each semicircle, equivalent to the reciprocal of the characteristic relaxation time ($1/\tau$). On the other hand these grain and grain boundary resistances can be identified by the magnitude of capacitance. The grain and grain boundary resistances from semi circles are presented in Fig. 1.4(b).

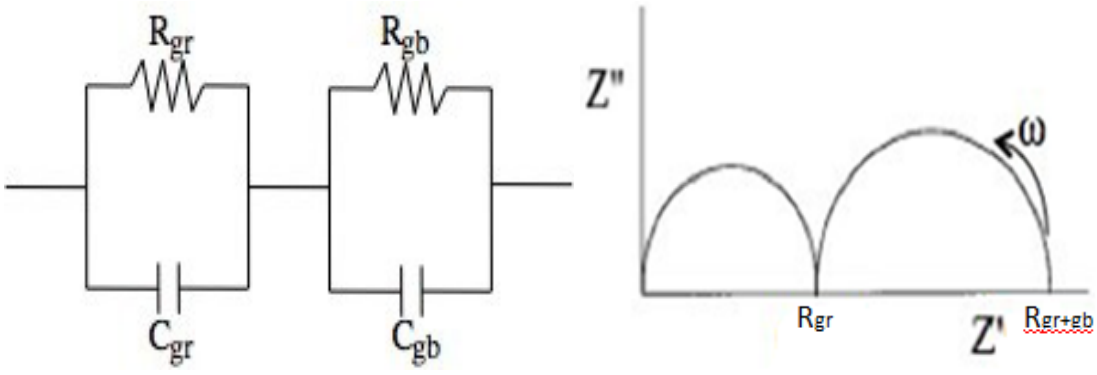

Fig.1.4 (a) an equivalent parallel circuit (b) impedance complex plane plot showing two semi circle components[10].

For the impedance data on CCTO at room temperature obtained by Sinclair et al. [10], it is clearly shown that there exists a non-zero resistance in the inset of Figure 1.5(a).

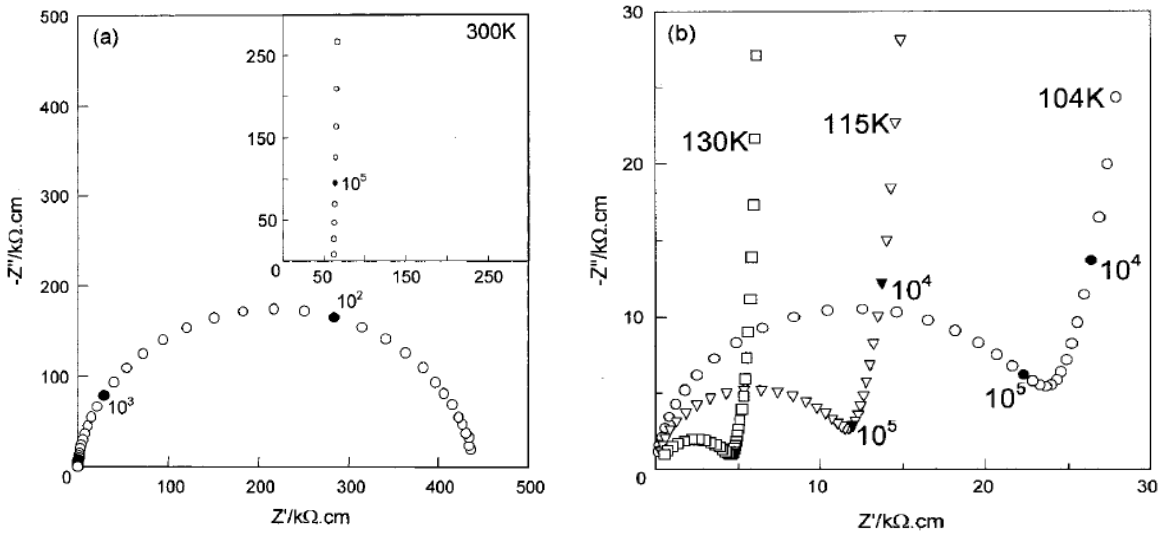

(a) (b)

Fig. 1.5 Complex impedance plane plot of CCTO (a) at 300 K (b) at lower temperature (104, 115, 130 K)[10].

Considering the semi circle at low frequency shown in the main figure, this result strongly indicates that there should be another semi circle at high frequency over 10^5 Hz. When the impedance plot was made below 130 K however the new data presented in Figure 1.5(b) confirmed the high frequency semi circle showing the grain resistance.

1.3 Ball milling:

Ball milling is a mechanical method. It is one of various types of comminution process. It is a process in which small particles are produced by reducing the size of larger ones by mechanical forces. It involves operations such as crushing, grinding and milling. Ball milling is the most common way to achieve this size reduction.

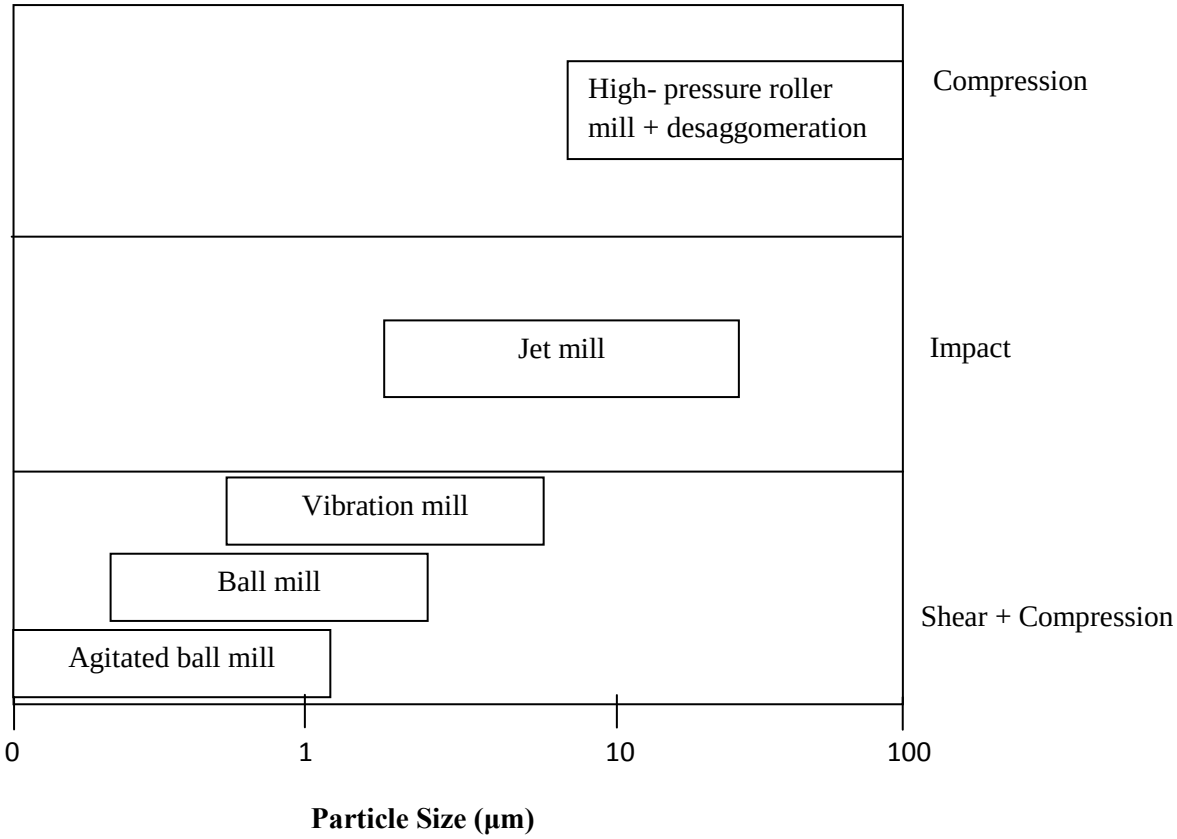

Fig. 1.6 Range of particle sizes reached with different types of mills.

One or more of a variety of mills may be used including high compression roller mills, jet mills (also referred to as fluid energy mills) and ball mills [11]. The high compression roller mills and jet mills achieve comminution without the use of grinding media. But in case of mills containing balls or rods comminution occurs by compression, impact and friction between the moving grinding media and the particles. Rod mills are not suitable for the production of fine powders whereas ball milling can be used to produce particle sizes from ~10 µm to as low as a fraction of a micrometer. Ball milling is suitable for wet or dry milling. Ball mills are categorized into various types depending on the method used to impart motion to the balls. In general we can divide ball milling into two types:-

a) High energy ball milling

b) Low energy ball milling

1.3.1 High energy ball milling:

High energy ball milling of powder particles as a method for materials synthesis has been developed as an industrial process to successfully produce new alloys and mixture in 1970. This powder metallurgical process allows the preparation of alloys and composites which cannot be synthesized via conventional routes.

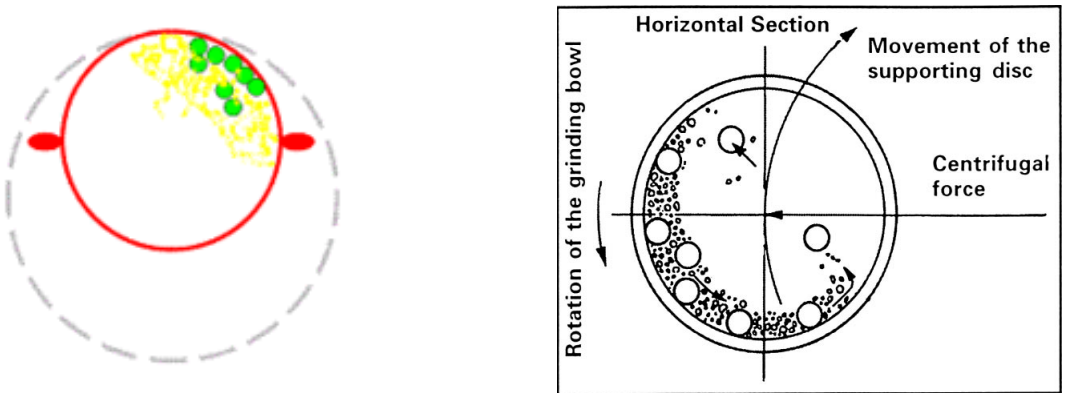

Fig. 1.7 Schematic of a high energy planetary ball mill[11].

In nano materials research this top down technique is well used to fine tune the grain sizes of the materials in nano scales. A variety of milling devices has been developed for different purposes including tumbler mills, attrition mills, shaker mills, vibratory mills, planetary mills etc. Here, grinding bowls rotates on their own axis while simultaneously rotating through an arc around the central axis. The grinding balls and the material in the grinding bowl are thus acted upon by the centrifugal forces which constantly change in direction and intensity resulting in efficient fast grinding process. The grinding bowl and the supporting disc rotate in opposite directions so that the centrifugal forces alternatively act in the same and opposite directions. This results in as a frictional effect the grinding balls running along the inner wall of the grinding bowl and impact effect the balls impacting against the opposite wall of the grinding bowl. The energy thus created by impact is many times higher than for traditional mills. This results in excellent grinding

performance and considerably shorter grinding times. Atmospheric contamination can be minimized by sealing the vial with flexible O ring after the powder has been loaded. If a milling medium a fluid (usually an organic fluid) is used contamination by the milling tools can be prevented and also it minimizes the wear. A few parameters exists in high energy ball milling which on changing we can produce a wide range of fine particles with different sizes and consequently with different physical properties. These parameters are

- Type of mill
- Milling atmosphere
- Milling media
- Intensity of milling
- Ball to powder weight ratio (BPR)
- Milling time
- Milling temperature

1.3.2 Low energy ball mill:

Low energy ball mills involve lower energy utilization. Tumbling ball mills usually referred to simply as ball mills consist of a slowly rotating horizontal cylinder that is partly filled with grinding balls and the particles to be ground. In addition to the factors discussed above the speed of rotation of the mill is an important variable since it influences the trajectory of the balls and the mechanical energy supplied to the powder. Defining the critical speed of rotation as the speed required to just take the balls to the apex of revolution we find that the critical speed is equal to $(g/a)1/2/(2\pi)$, where a is the radius of the mill and 'g' is the acceleration due to gravity. In practice ball mills are operated at ~ 75% of the critical speed so that the balls do not reach the top of the mill. In the milling process the objective is to have the balls fall onto the particles at the

bottom of the mill rather than onto the mill liner itself. For a mill operating at ~ 75% of its critical speed, this occurs for dry milling for a quantity of balls filling ~ 50% of the mill volume and for a charge of particles filling ~ 25% of the mill volume. For wet milling a useful guide is for the balls occupying ~ 50% of the mill volume and the slurry 40% of the mill volume with the solids content of the slurry equal to ~ 25-40%. Wet ball milling has an advantage over dry milling in that its energy utilization is somewhat higher (by ~ 10-20%). A further advantage is the ability to produce a higher fraction of finer particles. Disadvantages of wet milling are the increased wear of the grinding media the need for drying of the powder after milling and contamination of the powder by the adsorbed vehicle.

Ball milling is a fairly complex process that does not lend itself easily to rigorous theoretical analysis. We can define the energy utilization of the comminution method as the ratio of the new surface area created to the total mechanical energy supplied. In the milling process the particles experience mechanical stresses at their contact points due to compression, impact or shear with the mill medium or with other particles. The mechanical stresses lead to elastic and inelastic deformation and if the stress exceeds the ultimate strength of the particle to fracture of the particles. The mechanical energy supplied to the particle is used not only to create new surfaces but also to produce other physical changes in the particle (e.g., inelastic deformation, increase in temperature and lattice rearrangements within the particle). Changes in the chemical properties (especially the surface properties) can also occur especially after prolonged milling or under very vigorous milling conditions. Consequently the energy utilization of the process can be fairly low ranging from < 20% for milling produced by compression forces to < 5% for milling by impact. The rate of grinding is defined as the amount of new surface area created per unit mass of particles per unit time.

Fig. 1.8 Low energy ball milling

The rate of grinding also depends on the particle size. The rate decreases with decreasing particle size and as the particles become fairly fine (e.g. about 1μm to a few micrometers) it becomes more and more difficult to achieve further reduction in size. A practical grinding limit is approached (Fig 1.9). This limit depends on several factors. An important factor is the increased tendency for the particles to agglomerate with decreasing particle size. A physical equilibrium is therefore set up between the agglomeration and comminution processes. Another factor is the decreased probability for the occurrence of a comminution event with decreasing particle size. Finally the probability of a flaw with a given size existing in the particle decreases with decreasing particle size.

1.3.2.1 Ball Mill Features:

1) Stable performance, wearable

2) Equal product size

3) Low invest, low energy consumption

4) Easy and safe operation.

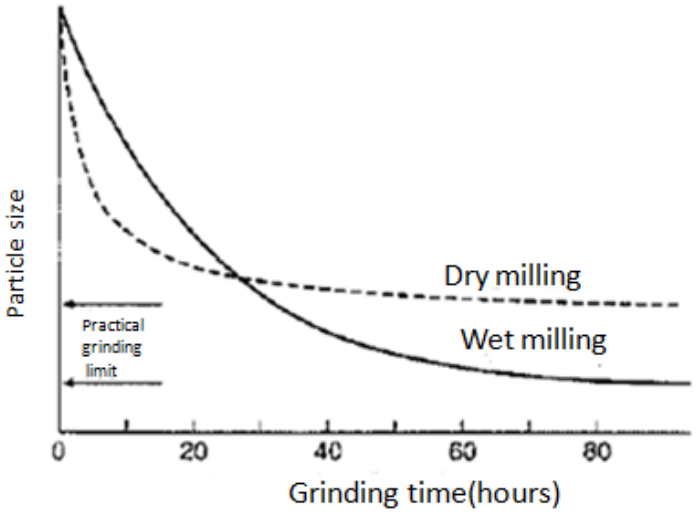

Fig. 1.9 Particle size versus grinding time for ball milling[12].

1.4 Calcination:

Calcination is a thermal treatment process applied to ores and other solid materials in order to bring about a thermal decomposition, phase transition or removal of a volatile fraction. The calcination process normally takes place at temperatures below the melting point of the product materials. Calcination is to be distinguished from roasting in which more complex gas solid reactions take place between the furnace atmosphere and the solids. Calcination is the intermediate step for the formation of ceramic in order to consolidate the material through conventional heating [13]. Calcination causes the constituents to interact by inter diffusion of their ions and so reduces the extent of the diffusion that must occur during sintering in order to obtain a homogeneous body. It can therefore be considered to be part of the mixing process. The calcination conditions are important factors controlling shrinkage during sintering. The required final phases may not be completely formed but the remaining chemical gradients may assist sintering. The main requirement is that calcination should yield a very consistent product. Calcination can be carried out by placing the mixed powders in shallow saggers in a batch or

continuous kiln. The saggers may need to be closed if any of the constituents are volatile as is the case with lead oxide. Container surfaces in immediate contact with the powder must not react with it both to avoid contamination and to permit reuse of the sagger. The thermal conductivity of powdered materials is always low so that a sufficiently uniform temperature can only be obtained through a depth of a centimeter when the period at maximum temperature is as is usual only 1 or 2 h. The conventional slow heating of the material is generally accomplished with the help of programmable controller at different rate of heating. Calcinations consist of different stages such as curing, evaporation, organic material removal, annealing in order to purify and to get a homogeneous body. Also it provides a very good yield of consistent product. The calcined material has usually undergone a limited amount of sintering and must be milled to give a powder or slip suitable for the shaping stage. The machinery and problems are essentially the same as those discussed above in relation to mixing. The calcine is usually coarser and more abrasive than the raw materials so that precautions against contamination are of more importance. The initial size reduction to produce suitable particles for the finer grinding processes can be carried out using any one of the wide range of pieces of equipment, jaw crushers, roller mills, hammer mills, mortar & pestle developed for ore dressing.

1.5 Green Forming:

Powder preparation stage is followed by shape forming stage. It is a process of giving a desired shape to powder by applying deforming forming forces such as pressing, casting etc. The desired goal of this step is the homogeneous packing of particles in the green body. Since the packing density controls the amount of shrinkage during firing the achievement of high packing density is also desirable. Prior to shape forming ceramic powders are mixed with processing additives [14]. The primary function of the binder is to give the dry shape sufficient strength to

survive the handling necessary between shaping and sintering. One of the most important requirements for a binder is that it should be possible to eliminate it from the compact without any disruptive effect.

The green forming techniques are as follows:

1.5.1 Dry Pressing:

It is the powder compaction method involving uniaxial pressure applied to the powder placed in a die between two rigid punches. It is effectively used for mass production of simple parts.

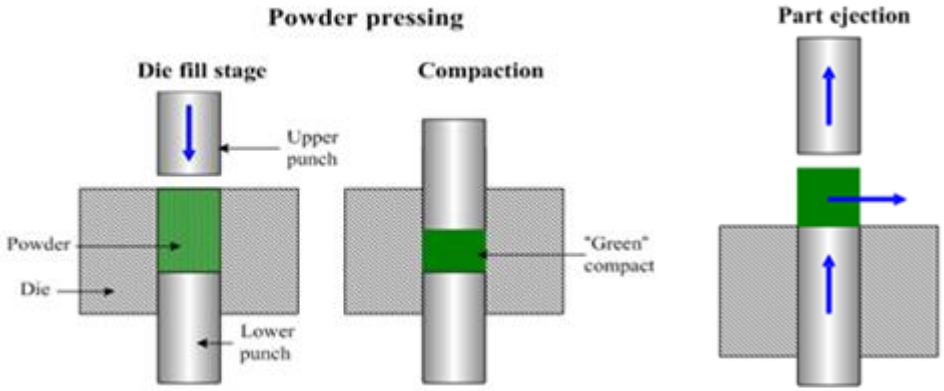

Fig. 1.10 Dry pressing[13].

Dry pressing is ideally suited to the formation of simple solid shapes and consists of three basic steps: filling the die, compacting the contents and ejecting the pressing solid. Pressure is applied uniaxially to the powder placed in a die between two rigid punches. The scheme of the dry pressing method is shown in the figure 1.10. In first step controlled amount of the powder is fed into the die cavity. Then upper punch moves down and presses the powder with a predetermined pressure. In last step green body is ejected from die. Die pressing which is conducted at the room temperature is called cold pressing. If the pressing process is conducted at

increased temperature it is called hot pressing. Die pressing is used for manufacturing insulating parts, magnetic ceramics, capacitors and substrates.

1.5.2 Cold isostatic pressing (CIP):

CIP is a type of isostatic pressing. In isostatic pressing pressure from multiple directions is applied through a liquid or gaseous medium surrounding the compacted part. CIP is conducted at room temperature. A flexible (commonly polyurethane) mold immersed in a pressurized liquid medium (commonly water) is used in the cold isostatic pressing method (figure 1.11). There are two types of cold isostatic pressing: wet bag and dry bag. In the wet bag method the mold is removed and refilled after each pressure cycle.

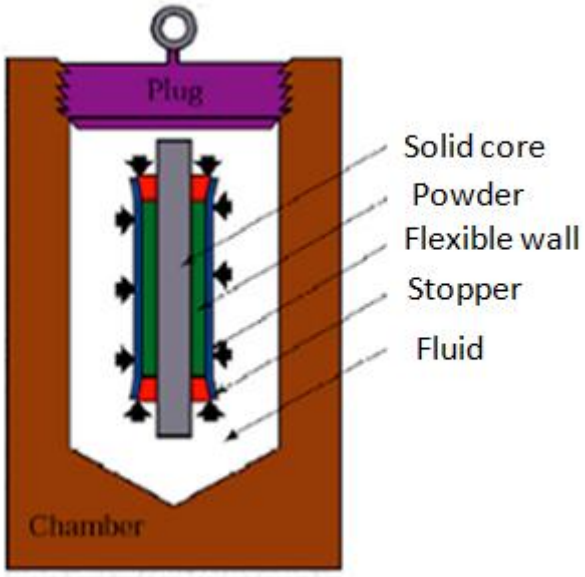

Fig. 1.11 Cold isostatic pressing

This method is suitable for compaction of large and complicated parts. In the dry bag method the mold is an integral part of the vessel. The dry bag method is used for compaction of simpler and

smaller parts. The CIP method has the following advantages as compared to the die cold pressing method:

- Better uniformity of compaction.
- More complex forms (for example long thin walled tubes) may be compacted.

1.6 Sintering:

Sintering (Firing) of ceramic materials is the method involving consolidation of ceramic powder particles by heating the green compact part to a high temperature below the melting point when the material of the separate particles diffuse to the neighboring powder particles. The driving force of sintering process is reduction of surface energy of the particles caused by decreasing their vapor- solid interfaces. This reduction in energy can be accomplished by atom diffusion processes that lead to either densification of the body by transport matter from inside the grains into the pores or coarsening of the microstructure by rearrangement of matter between different parts of the pore surfaces without actually leading to a decrease in the pore volume. Sintering is enhanced if a liquid phase takes part in the process (liquid phase sintering). Sintering process may be conducted in different atmospheres: air, inert atmosphere.

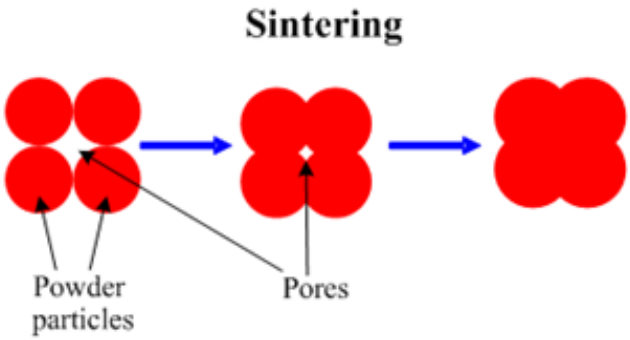

Fig. 1.12 Sintering Stages[15]

Sintering is a method for making objects from powder by heating the material in a sintering furnace [15] below its melting point (solid state sintering) until its particles adhere to each other. Sintering is traditionally used for manufacturing ceramic objects and has also found uses in such fields as powder metallurgy.

Fig. 1.13 Sintering furnace

A major problem during sintering is that the coarsening process reduces the driving force for densification. This interaction is sometimes expressed by the statement that sintering involves a competition between densification and coarsening. The domination of densifying diffusion processes will favor the production of a dense body. When coarsening processes dominate the production of a highly porous body will be favored [14]. Decrease of the porosity caused by the sintering process is determined by the level of the initial porosity of the green compact, sintering temperature and time. Sintering of pure oxide ceramics require relatively long time and high temperature because the diffusion proceeds in solid state. Applying pressure decreases sintering time and the resulted porosity. Tunnel kilns and periodic kilns are commonly used for ceramics sintering. In periodic kilns heating and cooling sintering stages are conducted according to a

prescribed procedure. In tunnel kilns the sintered parts are conveyed through different temperature zones.

Typical tunnel kiln has three zones:

1. Preheat zone for removing lubricant and other organic materials;
2. Sintering zone where the diffusion occurs;
3. Cooling zone where the sintered parts cool down.

1.6.1 Advantages of Sintering:

1. The possibility of very high purity for the starting materials and their great uniformity.
2. Preservation of purity due to the restricted nature of subsequent fabrication steps.
3. Stabilization of the details of repetitive operations by control of grain size in the input stages.
4. Absence of binding contact between segregated powder particles or inclusions (called stringering), as often occurs in melt processes.
5. No requirement for deformation to produce directional elongation of grains.
6. The possibility of creating materials of uniform controlled porosity.

1.7 Dielectric Materials:

A dielectric is an electrical insulator that may be polarized by the action of an applied electric field. When a dielectric is placed in an electric field, electric charges do not flow through the material as in a conductor but only slightly shift from their average equilibrium positions causing dielectric polarization: positive charges are displaced along the field and negative charges shift in the opposite direction. This creates an internal electric field which partly compensates the external field inside the dielectric[16]. If a dielectric is composed of weakly

bonded molecules those molecules not only become polarized but also reorient so that their symmetry axis aligns to the field.

While the term insulator refers to a low degree of electrical conduction, the term dielectric is typically used to describe materials with a high polarizability. The latter is expressed by a number called the dielectric constant. A common yet notable example is that a dielectric is the electrically insulating material between the metallic plates of a capacitor. The polarization of the dielectric by the applied electric field increases the capacitor's capacitance. The study of dielectric properties is concerned with the storage and dissipation of electric and magnetic energy in materials. Charge separation in a parallel plate capacitor causes an internal electric field. A dielectric (orange) reduces the field and increases the capacitance.

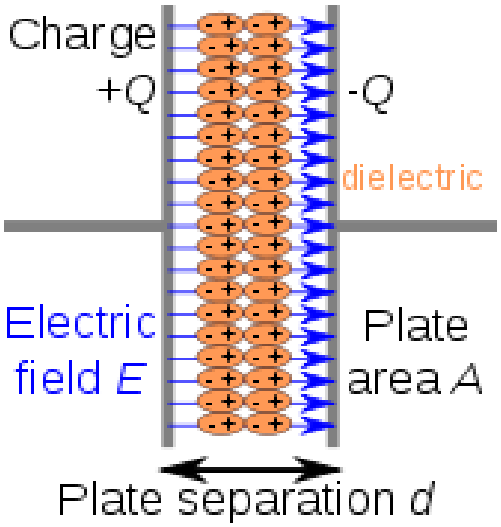

Fig. 1.14 Parallel plate capacitor[16].

1.8 Ceramic Processing:

We can divide the processing methods mainly into three groups depending on the state of starting precursors such as gaseous, liquidous or solidous. The table 1.1 shows the brief summery of these methods.

Table 1.1 Methods of ceramic processing

Starting materials	**Method**	**Product**
Gases	Chemical vapor deposition	Films, monoliths
Gas–liquid	Directed metal oxidation	Monoliths
Gas–solid	Reaction bonding	Monoliths
Liquid–solid	Reaction bonding	Monoliths
Liquids	Sol gel process	Films, fibers
	Polymer pyrolysis	Fibers, films
Solids (powders)	Melt casting	Monoliths
	Sintering of powders	Monoliths, films

1.9 Aim and Objectives of the present work:

The objective of this work is to study the effect of sintering temperature on dielectric properties of CCTO ceramic. This can be achieved by following steps:

1. Preparation of CCTO powder by Ball milling
2. Calcination of powder
3. Pressing of powder
4. Sintering of pellet
   4.1. Sintering temperature: 1025, 1050,1075 and 1100°C
   4.2. Sintering dwell time: 2 and 10 h
5. Characterizations
   5.1. X ray Diffraction
   5.2. Scanning Electron Microscopy
   5.3. Dielectric Measurement

CHAPTER 2

LITERATURE REVIEW

B. Barbier et al. [17] had reported synthesis of Dielectric properties of CCTO based ceramics and thick films (e ~50μm) prepared from powders synthesized by a chemical route method. The characteristics of pellets and thick films are compared. The pellets exhibit high values of the dielectric permittivity (ε_r ~1.4×10^5) and relatively small dielectric losses (tan δ ~0.16) at 1 kHz and room temperature. These properties are independent of the nature of the metallization of the electrodes. In addition, the dielectric permittivity decreases when the diameter of the electrodes of the pellets increases while the losses remain constant. This is strongly related to the nature of the dielectric material in between the electrodes constitutes a strong indication that the high dielectric permittivity values observed in this material are not related to an interfacial related mechanism but is an internal barrier layer capacitor type.

Jianjun Liu et al. [18] had reported synthesis of fine crystalline CCTO powder using wet chemistry method at relatively low temperatures and a shorter reaction time. The pure phase sample was obtained at 800°C for 0.5 h and the grain size of a pellet sample sintered at 1030°C for 4 h has a homogeneous distribution in the range of 0.4-1.5 μm. This method start with a homogeneous liquid solution of cation ingredients mixed in stoichiometric ratio at the atomic scale. Therefore, pure samples at the nanometer scale could theoretically be obtained at lower temperature and a shorter reaction time than that afforded by solid state reactions. In this method the metal oxides are formed in the first heat-treatment step and CCTO is produced by a subsequent solid state reaction.

Jianjun Liu et al. [19] have synthesized the giant dielectric constant material CCTO by pyrolyzing an organic solution containing stoichiometric amounts of the metal cations at a lower

temperature and a shorter reaction time than that for conventional solid state reaction. CCTO has a giant dielectric constant of up to 10^5 at room temperature and great potential for technological application. In this work, the two wet chemistry methods are reported to synthesize CCTO at relatively low temperatures and short reaction times. The pure phase sample was obtained at 800°C for 0.5 h, and the grain size of a pellet sample sintered at 1030°C has a homogeneous distribution in the range of 0.4-1.5 μm. The samples exhibit a giant dielectric constant of 11500. However this method still has the disadvantage that it involves handling chemicals in a glove box and refluxing of solutions.

Shuhua Jin et al. [20] synthesized CCTO by sol gel method. The novel nano ultrafine powders for the preparation of CCTO ceramic were prepared by the sol gel method and citrate auto ignition method. The relative dielectric constant of the ceramic sintered at 1000°C was measured with a magnitude of more than 10^4 at room temperature which was approaching to those of Pb containing complex perovskite ceramics and the loss tangent was less than 0.20 in a broad frequency region. The relative dielectric constant and loss tangent were also compared with that of CCTO ceramic prepared by other reported methods. Such CCTO ceramic prepared by the sol gel process with ideal electric properties is expected to find applications in electric devices.

Kim et al. [21] studies the micro structural evolution and dielectric properties of SiO_2 doped CCTO ceramics. The abnormal grain growth (AGG) behavior of undopped and SiO_2 doped CCTO ceramics were investigated. With the addition of 2 wt.% SiO_2 the AGG triggering temperature decreased from 1100 to 1060°C and the temperature for obtaining a uniform and coarse microstructure decreased from 1140 to 1100°C. The lowering of the AGG temperature by SiO_2 addition was attributed to the formation of a CuO-SiO_2 rich inter granular phase at lower

temperature. The apparent dielectric permittivity of coarse SiO_2 doped CCTO ceramics was ~10 times higher than that of fine SiO_2 doped CCTO ceramics at the frequency of 10^3-10^5 Hz. The doping of SiO_2 to CCTO ceramics provides an efficient route of improving the dielectric properties via grain coarsening. The correlation between the microstructure and apparent permittivity suggests the presence of a barrier layer near the grain boundary.

Wang et al. [22] synthesized Maxwell Wagner relaxation in CCTO/Ag composites. CCTO/Ag composites with different Ag weight fractions were prepared by sintering thoroughly mixed CCTO and Ag_2O powders at 1050°C in air. The samples were found to consist of Ag deficient insulating surface layers and Ag rich more conductive inner parts. Dielectric measurements reveal that apart from the distinct dielectric features for pure CCTO another dielectric relaxation appears near room temperature. This relaxation has been interpreted based on the Maxwell Wagner model due to discontinuity of the charge concentration across the interface between the surface and inner layers.

Zhu et al. [23] fabricated CCTO by oxalate coprecipitation method which is done at lower temperature and shorter reaction time than the conventional solid state reaction. The precipitation containing stoichiometric amounts of the metal cations was heat treated to achieve single phase CCTO. DTA/TGA was carried out on a dried precipitate to study the thermal decomposition process. The phases microstructure and dielectric properties of the sample were characterized by X ray diffraction, scanning electron microscopy and precision impedance analyzer.

Hutagalung et al. [24] synthesized CCTO by microwave assisted solid state reaction technique from $CaCO_3$, CuO and TiO_2 powders. Processing involved the preparation of raw material, mixing and milling, calcination, pellet forming and sintering processes. Conventional

furnace and microwave assisted sintering processes were employed in order to improve phase structures, morphology and dielectric properties of CCTO ceramics. Surface and fracture FESEM analysis showed that the microwave assisted sintered CCTO produced better densification and more uniform grain size compared to the conventional sintered sample.

Thomas et al. [25] synthesized nanoparticles of CCTO from a precursor route. A method of preparing the nano particles of CCTO with the crystallite size varying from 30 to 200 nm is optimized at a temperature as low as 680°C from the exothermic thermal decomposition of an oxalate precursor $CaCu_3(TiO)_4(C_2O_4)_8.9H_2O$. The phase singularity of the complex oxalate precursor is confirmed by the wet chemical analyses, X ray diffraction, FT-IR and TGA/DTA analyses. The UV is reflectance and ESR spectra of CCTO powders indicate that the Cu (II) coordination changes from distorted octahedra to nearly flattened tetrahedra to square planar geometry with increasing annealing temperature. The HRTEM images have revealed that the evolution of the microstructure in nanoscale is related to the change in Cu(II) coordination around the surface regions for the chemically prepared powder specimens. The nearly flattened tetrahedral geometry prevails for CuO_4 in the near surface regions of the particles whereas square planar CuO_4 groups are dominant in the interior regions of the nanoparticles. The powders derived from the oxalate precursor have excellent sinterability resulting in high density ceramics which exhibited giant dielectric constants upto 40000 (1 kHz) at 25°C accompanied by low dielectric loss < 0.07.

Kim et al. [26] studied neutron scattering study of anti ferromagetic order in CCTO. Magnetism in a single crystal CCTO has been studied using elastic and inelastic neutron scattering. He has measured the order parameter of the anti ferromagnetic phase transition at T_N = 24.1(1) K. The observed magnetic structure can be consistently described by spins ordered

collinearly along crystallographic direction. A spin wave mode of ω=7.3 meV has been observed and compared with a linear spin wave theory.

Chivalrat Masingboon et al. [27] nano sized powders of CCTO were synthesized by a polymerized complex method and calcined at 600, 700 and 800°C in air for 8 h. The diameter of the powders ranges from 30 to 100 nm. The CCTO powders were characterized by TG-DTA, XRD, FTIR, SEM and TEM. Sintering of the powders was conducted in air at 1100°C for 16 h. The XRD results indicated that all sintered samples have a typical perovskite CCTO structure with some amount of $CaTiO_3$ and CuO. SEM micrographs of the sintered CCTO ceramics showed the average grain size of 10-15μm. The samples exhibit a giant dielectric constant ε' of 10000–20000. It is found that ε is independent on the frequency and weakly dependent on temperature. The Maxwell Wagner polarization mechanism is used to explain the high permittivity in these ceramics. It is also found that all three sintered samples have the same activation energy of grains which is 0.116 eV. On the other hand the activation energy of grain boundaries is found to be 0.219, 0.391 and 0.641 eV for CCTO ceramics prepared using the CCTO powders calcined at 600, 700 and 800°C, respectively.

Jha et al. [28] synthesized CCTO by polymeric citrate precursor route. Using citric acid and ethylene glycol a polymeric precursor of the above compound was obtained at low temperatures (135°C) which on subsequent heat treatments led to pure CCTO at 1000°C. On sintering further at 1000°C (20 h) the disks show high density (98%) and the dielectric constant was of the order of 3000 at 1 kHz. The dielectric loss varies between 0.3 and 0.35 till 100 kHz beyond that it increases sharply from 0.35 to 0.7 in the frequency range of 100-500 kHz. Our studies on dielectric properties of the above oxide synthesized by the ceramic method and sintered under the same conditions led to a dielectric constant of around 2200 at 1 kHz. The

dielectric constant decreases with frequency in the oxides obtained by either of the above methods. SEM show much larger grains of 2-4 μm in the solid obtained by the ceramic route while the grains were much smaller (0.5-1.0 μm) in the oxide prepared by the polymeric citrate precursor route.

Smith et al. [29] synthesized low loss colossal dielectric CCTO by an anion substitution route. An anion substitution route was utilized for lowering the dielectric loss in CCTO by partial replacement of oxygen by fluorine. This substitution reduced the dielectric loss and retained a high dielectric constant that was essentially temperature independent from 25 to 200°C. In particular $CaCu_3Ti_4O_{11.7}F_{0.3}$ exhibited a giant dielectric constant over 6000 and low dielectric loss below 0.075 at 100 kHz within a temperature range of 25-200°C. Flourine analysis confirmed the presence of fluorine in all samples measured.

Liu et al. [30] fabricated electrical hoterogeneity of CCTO by sol gel method. Using tetrabutyl titanate calcium nitrate and copper nitrate a gel of these compounds was obtained at room temperature which on subsequent heat treatments led to CCTO powder at 900°C for 1 h. On sintering further at 1060°C for 48 h the dielectric constant of CCTO ceramics is above 35000 at 1 kHz and it displays a good tune behavior. Impedance spectroscopy on CCTO ceramics demonstrates that they are electrically heterogeneous and consist of semiconducting grains with insulating grain boundaries. The dc bias experiment demonstrates clearly that the grain boundary response is consistent with a Schottky barrier response. Therefore CCTO ceramics display an internal barrier layer capacitor (IBLC) behavior.

Subramanian et al. [31] reported valence degeneracy in CCTO. The synthesis of CCTO has been accomplished at a pressure of 60 kbar. Analysis of single crystal X ray diffraction data demonstrates that this compound is isostructural with CCTO. The electrical resistivity data for

CCTO show metallic behavior and the magnetic susceptibility indicates delocalized electrons for both Cr and Cu. The Cu–O and Cr–O bond distances give fractional valences of $Cu^{2.45}$ and $Cr^{3.66}$, thus indicating both Cu and Cr 3d states at the Fermi level.

Chiodelli et al. [32] reported Electric and dielectric properties of pure and doped CCTO perovskite materials. AC impedance spectroscopy measurements were performed in the 15-700 K temperature range on pure and Ni, Fe and Co doped CCTO materials. Capacitance values were also confirmed by direct current measurements at room temperature. Thermoelectric power measurements showed that the electrons are involved in the conduction process of the semiconducting bulk region. The IS results evidenced a dielectric behaviour in the grain boundary region giving a permittivity of about 3400 for the pure sample so CCTO can be considered an internal barrier layer capacitance (IBLC) material. The giant permittivity of CCTO can be strongly increased to values of $15x10^4$ by Co doping on Ti site. The IBLC behaviour together with the giant permittivity and the opportunity to combine capacitance and resistance values in an R‖C circuit evidence the applicability of this material as an integrated resonant element for the electronic industry.

Yu et al. [33] synthesized single phase cubic perovskite CCTO powders by microwave heating with a relatively low energy consumption and short time compared with conventional synthesis. The reaction evolution of forming CCTO has been suggested according to the XRD data. The ceramics from microwave synthesized powder was found to have higher dielectric constant than that from conventional synthesized powder under the same sintering conditions.

Hutagalung et al. [34] studied microwave assisted sintering of CCTO. CCTO electroceramic was prepared by a microwave assisted solid state reaction technique from $CaCO_3$, CuO and TiO_2 powders. Processing involved the preparation of raw material, mixing and

milling, calcination, pellet forming and sintering processes. Conventional furnace and microwave assisted sintering processes were employed in order to improve phase structures, morphology and dielectric properties of CCTO ceramics. Surface and fracture FESEM analysis showed that the microwave assisted sintered CCTO produced better densification and more uniform grain size compared to the conventional sintered sample.

Hutagalung et al. [35] studied the role of tin oxide addition on the properties of microwave treated CCTO. A microwave (MW) irradiation process was performed to pre-sintered CCTO. A conventional furnace was used for calcination as well as for the sintering processes whilst a domestic microwave oven was employed for MW irradiation in order to produce better morphology improved phase structures and dielectric properties of CCTO products. SEM analysis shows that the microstructures of MW irradiated samples are denser with larger grain size if compared to the untreated samples. Dielectric properties also have been improved by MW treatment with higher dielectric constant and lower dielectric loss. Meanwhile the addition of tin oxide (SnO_2) to CCTO provides strong effects on the dielectric constant of both without and with MW irradiated samples. It was found that the dielectric constant of CCTO decreases exponentially with mole percentages of SnO_2. However, the addition of SnO_2 shows better dielectric loss properties of CCTO.

Tselev et al. [36] investigated the dielectric response of CCTO thin films grown epitaxially on $LaAlO_3$ (001) substrates by pulsed laser deposition. The dielectric response of the films was found to be strongly dominated by a power law in frequency typical of materials with localized hopping charge carriers in contrast to the Debye like response of the bulk material. The film conductivity decreases with annealing in oxygen and it suggests that oxygen deficit is a cause of the relatively high film conductivity. With increase of the oxygen content the room

temperature frequency response of the CCTO thin films changes from the response indicating the presence of some relatively low conducting capacitive layers to purely power law and then toward a frequency independent response with a relative dielectric constant $\varepsilon' = 10^2$. The film conductance and dielectric response decrease upon decrease of the temperature with dielectric response being dominated by the power law frequency dependence. Below 80 K the dielectric response of the films is frequency independent with ε' close to 10^2. The results provide another piece of evidence for an extrinsic Maxwell Wagner type origin of the colossal dielectric response of the bulk CCTO material connected with electrical inhomogeneity of the bulk material.

Shao et al. [37] have prepared CCTO ceramics by the conventional solid state reaction method under various sintering temperatures from 1000 to 1120°C at a interval of 10°C. Microstructures and crystalline structures were examined by scanning electronic microscopy and X ray diffraction, respectively. It has been reported that the morphologies change significantly with the sintering temperature. Ceramic specimens prepared by this method have a good polycrystalline structure in spite of the different microstructures. The dielectric permittivity was found to increase with the sintering temperature and is closely related to the polycrystalline microstructure particularly to the grain size. This suffers from the disadvantages of inhomogeneity and it also require repetitive grinding and firing at high temperatures and long reaction time.

CHAPTER 3

EXPERIMENTAL WORK

CCTO was prepared by using conventional solid state reaction method:

$$CaCO_3 + 3CuO + 4TiO_2 \rightarrow CaCu_3Ti_4O_{12} + CO_2 \uparrow$$

High purity $CaCO_3$ (99.98%), CuO (99.9%) and TiO_2 (99.95%) were used as the starting materials. These raw materials were mixed in stoichiometric amounts using agate mortar. Total weight of the mixture was 100 gms. The raw powders were mixed by using Fritsch Planetary micro ball mill with zirconia media in pulverisette deionized water for 24 h. Put this liquid in a furnace upto 350°C. This sample was grinded to give a mixed powder after making its cake and subsequently it was calcined at 1000 K for 24 h. PVA was added into the powders as organic binder to help the formation of cylindrical compacts of 12 mm in diameter and 2-3 mm in height under a uniaxial pressure of 220 Kg/cm^2. PVA was volatilized at 600°C and the compacts were sintered at temperatures in the range from 1025 to 1100°C for 2 and 10 h. Phase evaluation was done using X ray powder (XRD). XRD was done in 2θ range between 20- 80° for 22 minutes. XRD showed that the compound crystallizes in a cubic perovskite related structure with lattice parameter a = 0.7391 nm. The microstructure was evaluated by scanning electron microscopy (SEM). The dielectric properties and impedance analysis of the present ceramics were determined using the Impedance analyzer in the frequency range from 10^2 Hz to 10^7 Hz.

3.1 Calculations:

1) For initial concentrations

$$CaCO_3 + 3CuO + 4TiO_2 \longrightarrow CaCu_3Ti_4O_{12} + CO_2$$

Weight of $CaCO_3$ = 1 x 40.08 + 1 x 12.01 + 3 x 16
= 100.09 g

Weight of CuO = 1 x 63.55 + 1 x 16
= 79.55 g

Weight of TiO_2 = 47.87 + 16 x 2
= 79.88 g

Weight of $CaCu_3Ti_4O_{12}$ = 1 x $CaCO_3$ + 3 x CuO + 4 x TiO_2
= 100.09 + 238.65 + 319.60
= 614.27g

For 1 mol of CCTO 1 mol of $CaCO_3$, 3 mol of CuO and 4 mol of TiO_2 required.

→ for 614.27 g of CCTO ,658.27 g of mixture was required

→ For 200 g of CCTO , 214.2 g of mixture was required

Weight of $CaCO_3$ required = 32.4 g

Weight of CuO required = 77.6 g

Weight of TiO_2 required = 104.0 g

2) For PVA

3% PVA solution is there

2% PVA is to be added.

→ weight of PVA = 1.238

100 ml of PVA solution →3 g

→ 3g → 100ml

→ 1g → 100/3ml

→1.2384 → 41.2 ml ~ 41 ml

→ Volume of PVA to added = 41 ml

3.2 Calcination:

The ball milled powders were calcined at 1000°C for 24 h to remove the volatile materials. The calcination schedule is shown in fig. 4.5.

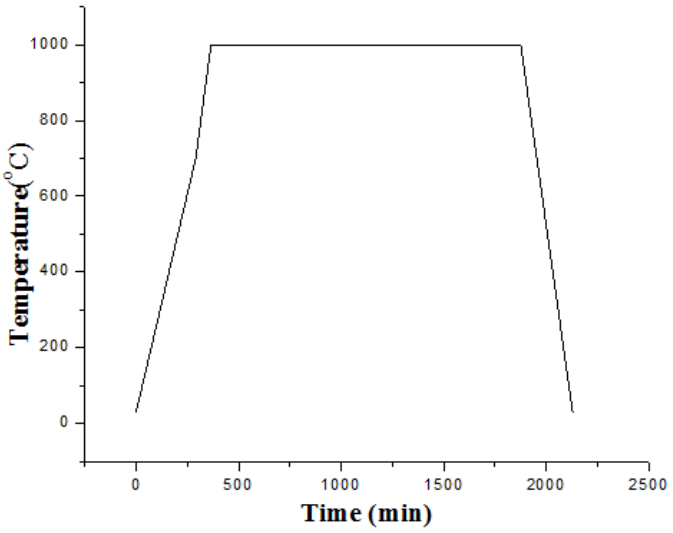

Fig 3.1 Calcination schedule for ball milled samples

3.3 Pressing:

The calcined powder was grinded by a grinder and then sieved using a 75 micron sieve before pressing. It is necessary to provide the binding force among the calcined particles in order to make a green ceramic pellet of CCTO. With the dried powder approximately 3 wt% of polyvinyl alcohol (PVA) was mixed. After mixing the aggregate of CCTO powder and PVA was dried in a drying oven for minimum 30 minutes. They were pressed into pellets under a pressure of 210 kg/cm^2. The powder was uniaxially pressed at 200 MPa into discs of 12 mm in diameter and 3 mm in thickness.

3.4 Sintering:

Conventional sintering was done at 1025, 1050, 1075 and 1100°C for holding time of 2 h, 10 h. Initially heating rate was kept slow (1°C /min) until temperature reaches 100°C and 2°C/min up to 400°C. Increased rates were up to 3°C/min and 4°C/min at higher temperature. Conventional sintering schedule is shown in figure at different temperatures.

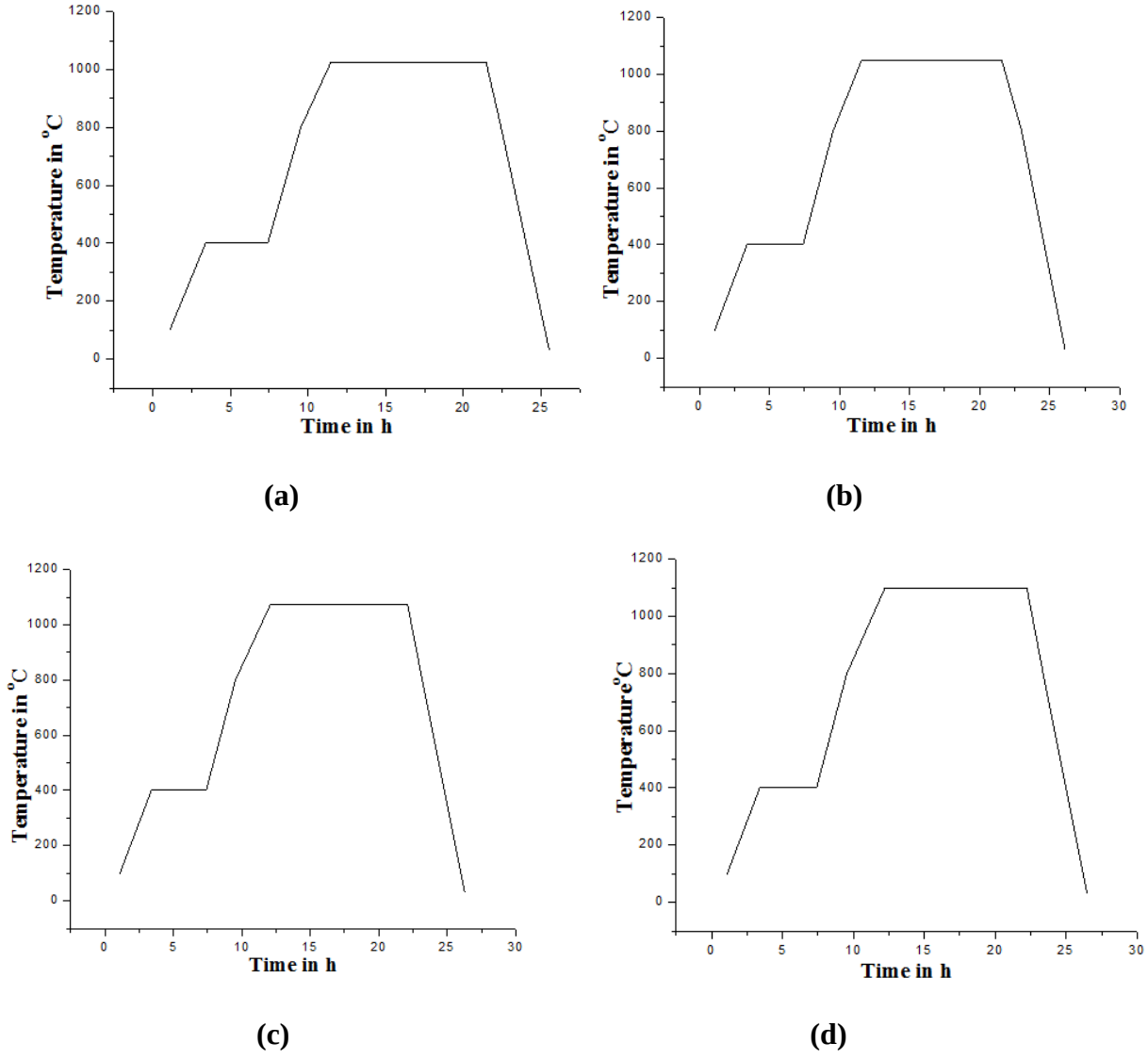

Fig 3.2 Conventional Sintering schedule at (a) 1025, (b) 1050, (c) 1075, (d) 1100°C

CHAPTER 4

CHARACTERIZATION TECHNIQUES

4.1 Scanning electron microscope:

The scanning electron microscope (SEM) is a type of electron microscope that images the sample surface by scanning it with a high energy beam of electrons in a raster scan pattern. The electrons interact with the atoms that make up the sample producing signals that contain information about the sample's surface topography, composition and other properties such as electrical conductivity. The figure 4.1 shows the components of SEM [37]. In a typical SEM electrons are thermionically emitted from a tungsten or lanthanum hexa boride (LaB_6) cathode and are accelerated towards an anode; alternatively electrons can be emitted via field emission (FE).

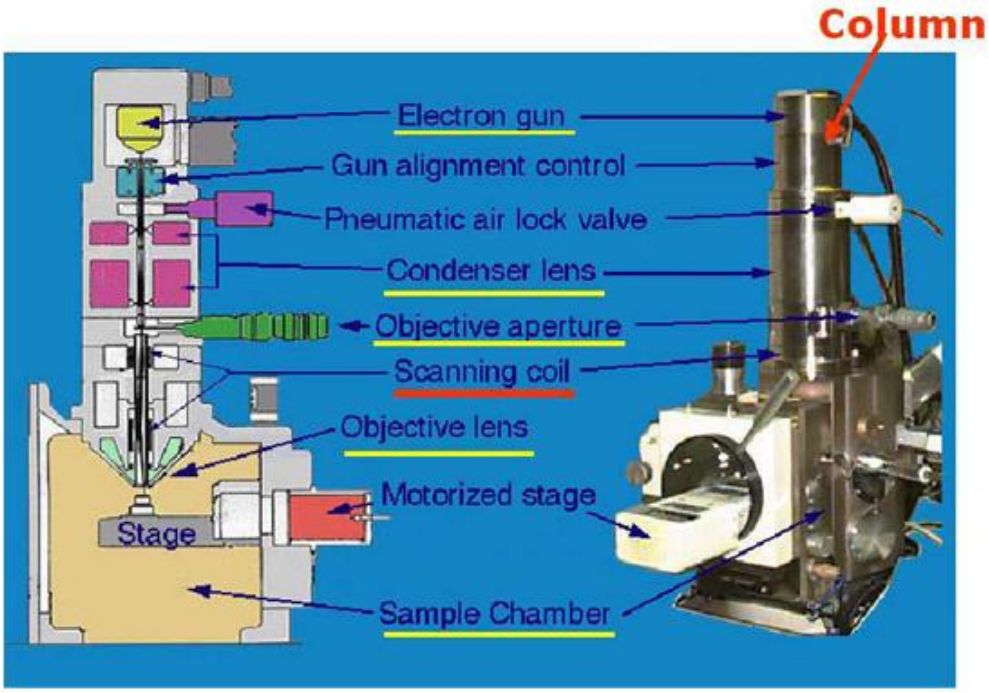

Figure 4.1 Basic Components of SEM[38].

The electron beam which typically has an energy ranging from a few hundred eV to 100 keV is focused by one or two condenser lenses into a beam with a very fine focal spot sized 0.4 nm to 5 nm. Tungsten is used because it has the highest melting point and lowest vapour pressure as compared to other metals thereby allowing it to be heated for electron emission. The types of signals produced by an SEM include secondary electrons back scattered electrons (BSE), characteristic X rays, light, specimen current and transmitted electrons. Secondary electron detectors are common in all SEMs but it is rare that a single machine would have detectors for all possible signals. The signals result from interactions of the electron beam with atoms at or near the surface of the sample. In the most common or standard detection mode secondary electron imaging or SEI the SEM can produce very high resolution images of a sample surface revealing details about less than 1 to 5 nm in size. Due to the very narrow electron beam SEM micrographs have a large depth of field yielding a characteristic three dimensional appearance useful for understanding the surface structure of the samples. A wide range of magnifications is possible from about 10 times about equivalent to that of a powerful hand lens to more than $5x10^5$ times about 250 times the magnification limit of the best light microscopes. Back scattered electrons (BSE) are beam electrons that are reflected from the sample by elastic scattering. BSE are often used in analytical SEM along with the spectra made from the characteristic X rays. Because the intensity of the BSE signal is strongly related to the atomic number of the specimen BSE images can provide information about the distribution of different elements in the sample. For the same reason BSE imaging can image colloidal gold immune labels of 5 or 10 nm diameter which would otherwise be difficult or impossible to detect in secondary electron images in biological specimens. Characteristic X rays are emitted when the electron beam removes an inner shell electron from the sample causing a higher energy electron to fill the shell and release energy.

These characteristic X rays are used to identify the composition and measure the abundance of elements in the sample.

Figure 4.2 Zeiss EVO MA 10 SEM at NPL, New Delhi

The beam passes through pairs of scanning coils or pairs of deflector plates in the electron optical column typically in the objective lens which deflect the beam horizontally and vertically so that it scans in a raster fashion over a rectangular area of the sample surface. When the primary electron beam interacts with the sample the electrons lose energy by repeated scattering and absorption within a tear drop shaped volume of the specimen known as the interaction volume which extends from less than 100 nm to around 5 μm into the surface. The size of the interaction volume depends on the electrons landing energy, the atomic number of the specimen and the specimen's density. The emission of electrons and electromagnetic radiations which can be detected to produce an image. The spatial resolution of the SEM depends on the size of the electron spot which in turn depends on the magnetic electron optical system which

produces the scanning beam. The resolution is also limited by the size of the interaction volume or the extent to which the material interacts with the electron beam. The spot size and the interaction volume both might be large compared to the distances between atoms so the resolution of the SEM is not high enough to image individual atoms as is possible in the transmission electron microscope. Depending on the instrument the resolution can fall somewhere between 1 nm and 20 nm. The figure 4.2 shows Zeiss EVO MA 10 SEM used at NPL, New Delhi.

4.2 X ray diffraction:

X ray diffraction (XRD) is a material characterization technique that can be useful for analyzing the lattice structure of a material. XRD is a nondestructive method for the structure analysis of crystals. The sample is irradiated with monochromatic X ray light and the stray radiation recorded. An important field of application is the identification of crystalline fractions in powders. The X ray radiation most commonly used is that emitted by copper whose characteristic wavelength for the K radiation is =1.5418 A°. When the incident beam strikes a powder sample diffraction occurs in every possible orientation of 2θ. The diffracted beam may be detected by using a moveable detector such as a Geiger counter which is connected to a chart recorder. In normal use the counter is set to scan over a range of 2θ values at a constant angular velocity. Routinely a 2θ range of 5 to 80 degrees is sufficient to cover the most useful part of the powder pattern. The scanning speed of the counter is usually 2θ of 2° /min and therefore about 30 minutes are needed to obtain a trace.

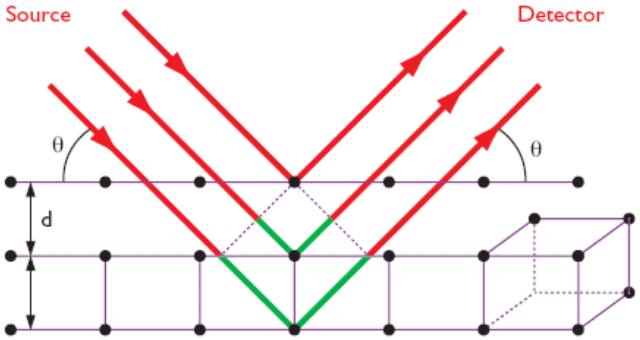

Figure 4.3 basic process of XRD

4.2.1 Features:

- X ray measurements of powders are easily performed, they are nondestructive and only small quantities (approx. 2 mg) are needed. The samples may be of different form:
  - powder between foils in transmission
  - powder in capillaries in transmission
  - plane-parallel pieces in reflection
  - layers on substrates in reflection
- Bulk samples must have particular dimensions, they must be plane parallel and smooth, amorphous fractions are not analysed.
- Crystallite sizes between 20 and 1000A$^{\circ}$ can be calculated from the half widths according to the Scherrer formula.
- Lattice constants can be refined to determine e.g. stoichiometries according to the Vegard formula.
- Structure controls and structure determinations can be performed with the Rietveld program.
- Simple texture measurements of layers on substrates can be rapidly carried out using position sensitive detectors.

4.2.2 Basic principles of XRD:

XRD analysis uses the property of crystal lattices to diffract monochromatic X ray light. This involves the occurrence of interferences of the waves scattered at the successive planes which are described by Bragg's equation:

$$n\lambda = 2\,d\sin\theta \quad (n = 1,2,3,...) \qquad \ldots(4.1)$$

where, λ is the wavelength, n is order of diffraction, d is the lattice plane distance and θ is half the diffraction angle. This relation is used for the structure analysis of crystals.

From XRD pattern we can find average size of crystals by Schherer's formula

$$D = \frac{0.9\lambda}{\beta\cos\theta} \qquad \ldots(4.2)$$

Where, β is full width half maximum (FWHM), λ is the wavelength used and D is the Crystalline size. This formula is valid for up to 100 nm size only. The figure 4.4 shows Philips PW 3710 Powder X ray Diffractometer used for XRD analysis of samples.

- In diffractograms of powders not free from phase shift several diffraction patterns of different crystalline fractions can be superimposed. The detector is a position sensitive proportional counter for high speed recording or a scintillation counter for better angular resolution. Instruments that work on this principle are called diffractometers.

- By accurately measuring peak positions over a long range of 2theta, you can determine the unit cell lattice parameters of the phases in your sample

- Sealed X ray tubes tend to operate at 1.8 to 3 kW.

- The unit cell is the basic repeating unit that defines a crystal.

Figure 4.4 Philips PW 3710 Powder X ray Diffractometer

4.3 Dielectric spectroscopy:

Dielectric spectroscopy also known as Electrochemical Impedance Spectroscopy measures the dielectric properties of a medium as a function of frequency[37- 40]. It is based on the interaction of an external field with the electric dipole moment of the sample often expressed by permittivity.

It is also an experimental method of characterizing electrochemical systems. This technique measures the impedance of a system over a range of frequencies and therefore the frequency response of the system including the energy storage and dissipation properties is revealed. Often data obtained by EIS is expressed graphically in a Bode plot or a Nyquist plot.

Impedance is the opposition to the flow of alternating current (AC) in a complex system. A passive complex electrical system comprises both energy dissipater and energy storage

elements. If the system is purely resistive then the opposition to AC or direct current (DC) is simply resistance. Almost any physicochemical system such as electrochemical cells mass beam oscillators and even biological tissue possesses energy storage and dissipation properties. EIS examines them.

This technique has grown tremendously in stature over the past few years and is now being widely employed in a wide variety of scientific fields such as fuel cell testing, biomolecular interaction and microstructural characterization. Often EIS reveals information about the reaction mechanism of an electrochemical process: different reaction steps will dominate at certain frequencies and the frequency response shown by EIS can help identify the rate limiting step.

4.3.1 Dielectric Mechanism:

In general dielectric mechanisms can be divided into relaxation and resonance processes. The most common depend on frequencies are:

4.3.1.1 Electronic polarization:

This resonant process occurs in a neutral atom when the electric field displaces the electron density relative to the nucleus it surrounds. This displacement occurs due to the equilibrium between restoration and electric forces. Electronic polarization may be understood by assuming an atom as a point nucleus surrounded by spherical electron cloud of uniform charge density.

4.3.1.2 Atomic polarization:

Atomic polarization is observed when the electronic cloud is deformed under the force of the applied field so that the negative and positive charges are formed. This is a resonant process.

4.3.1.3 Dipole relaxation:

This originates from permanent and induced dipoles aligning to an electric field. Their orientation polarization is disturbed by thermal noise which misaligns the dipole vectors from the direction of the field and the time needed for dipoles to relax is determined by the local viscosity. These two facts make dipole relaxation heavily dependent on temperature and chemical surrounding.

4.3.1.4 Ionic relaxation:

Ionic relaxation comprises ionic conductivity and interfacial and space charge relaxation. Ionic conductivity predominates at low frequencies and introduces only losses to the system. Interfacial relaxation occurs when charge carriers are trapped at interfaces of heterogeneous systems. A related effect is Maxwell Wagner Sillars polarization where charge carriers blocked at inner dielectric boundary layers on the mesoscopic scale or external electrodes on a macroscopic scale lead to a separation of charges. The charges may be separated by a considerable distance and therefore make contributions to the dielectric loss that are orders of magnitude larger than the response due to molecular fluctuations [38].

4.3.1.5 Dielectric relaxation:

Dielectric relaxation as a whole is the result of the movement of dipoles (dipole relaxation) and electric charges (ionic relaxation) due to an applied alternating field and is usually observed in the frequency range 10^2-10^{10} Hz. Relaxation mechanisms are relatively slow compared to resonant electronic transitions or molecular vibrations which usually have frequencies above 10^{12} Hz.

4.4 Measurement Techniques:

4.4.1 Density measurement:

The diameters and thicknesses of the pellets were measured using vernier calipers with least count 0.05mm. The samples were weighed on electronic scale capable of measuring 1mg at least. The density was calculated according to the formula

$$D = \frac{\pi}{\left(\pi d^2 / 4\right)[t]} \qquad \ldots(4.4)$$

where, m is mass, d is diameter and t thickness of the pellet.

4.4.2 Measurement of dielectric properties:

In order to measure the dielectric constant and the loss tangent of CCTO pellets, it is necessary to make the both surfaces of ceramic samples conductive. For this purpose, each pellets were coated with silver paste. For better adhesion pellets were then dried for 30 minutes at 200°C. The dielectric properties were studied using Novocontrol made Alpha A High Performance frequency Analyser.

5.1 Calcination:

The XRD of the calcined powder is given below. XRD pattern matched with standard CCTO XRD pattern. This is in agreement with many researchers that finer the particle lesser the calcination time.

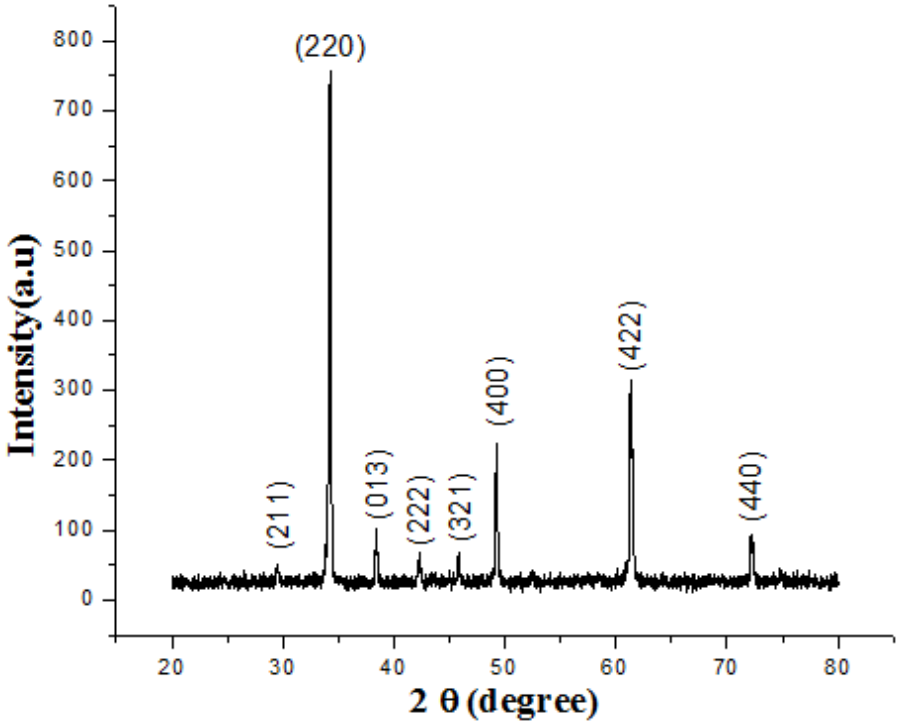

Fig 5.1 XRD pattern of Calcined CCTO powder

5.2 X ray Diffraction Analysis:

The XRD pattern of calcined powder is shown in figure.

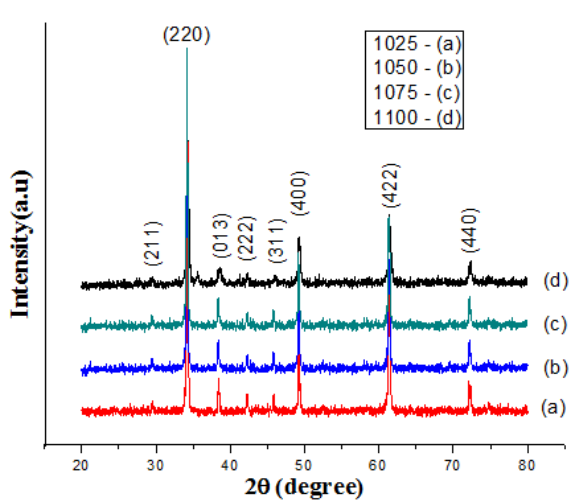

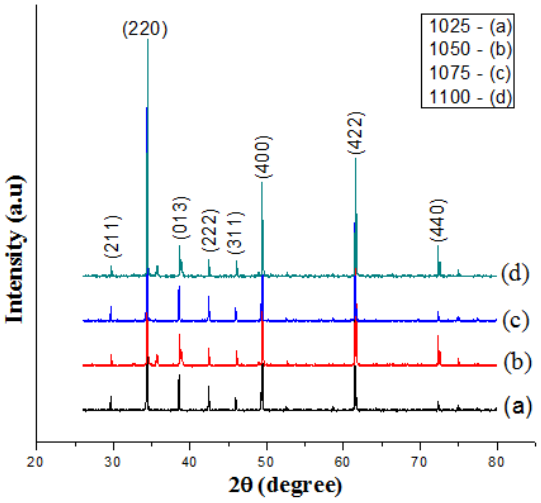

Fig. 5.2 XRD pattern of CCTO sintered for 2 h **Fig. 5.3 XRD pattern of CCTO sintered for 10 h**

This XRD patterns of experimental data match with the standard XRD JCPDF No. 75-2188. Lattice parameter of our specimen is found ~ 7.391A°. This figure shows that sintering temperature does not affect the XRD pattern or composition of CCTO. The diffraction peaks are indexed to a body centered cubic perovskite related structure of space group Im3. It indicates that all of the ceramic specimens prepared in the present study have a good polycrystalline structure. However, the heating time period enhances the sharpness of XRD peaks and decreases the disordering as shown in fig. 5.2 and fig. 5.3.

5.2 Scanning electron microscope (SEM) analysis:

SEM images of surface morphologies of the pure CCTO and sintered at 1025°C is shown in fig 5.4. CCTO does not have perfectly formed grains but it is found in agglomerated form. The biggest grain size is 13 μm while smallest one is 8 μm. It could be clearly observed that the agglomerates are actually formed from very small particle in submicron range size.

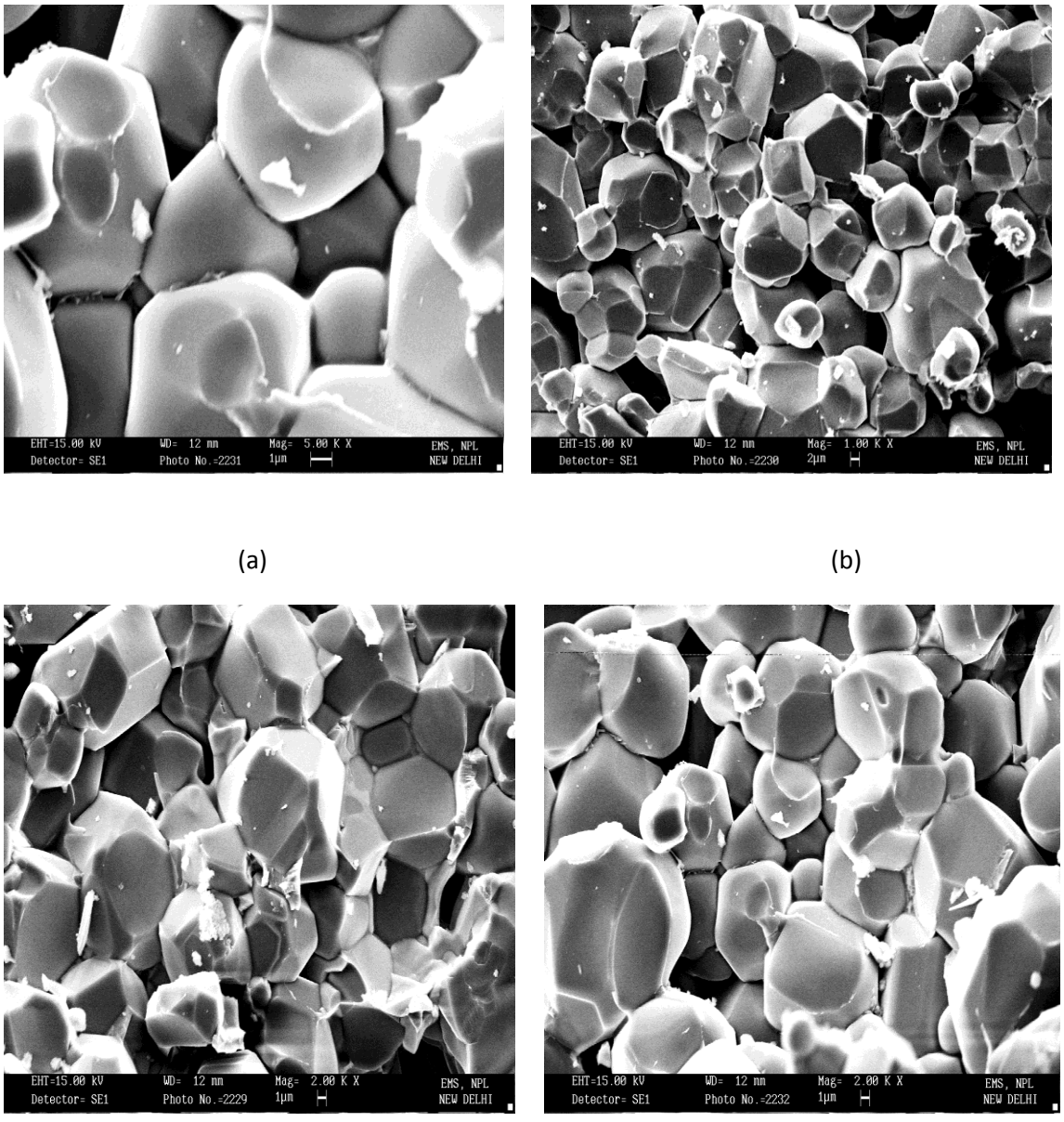

Fig. 5.3 SEM micrograph of CCTO sintered at 1025°C at different magnifications.

SEM micrograph of CCTO sintered at 1050°C for 10 h is given in fig 5.4. No additional phase is present in it and there is less amount of fracture grains. The biggest grain size is 17 μm while the smallest one is 8 μm.

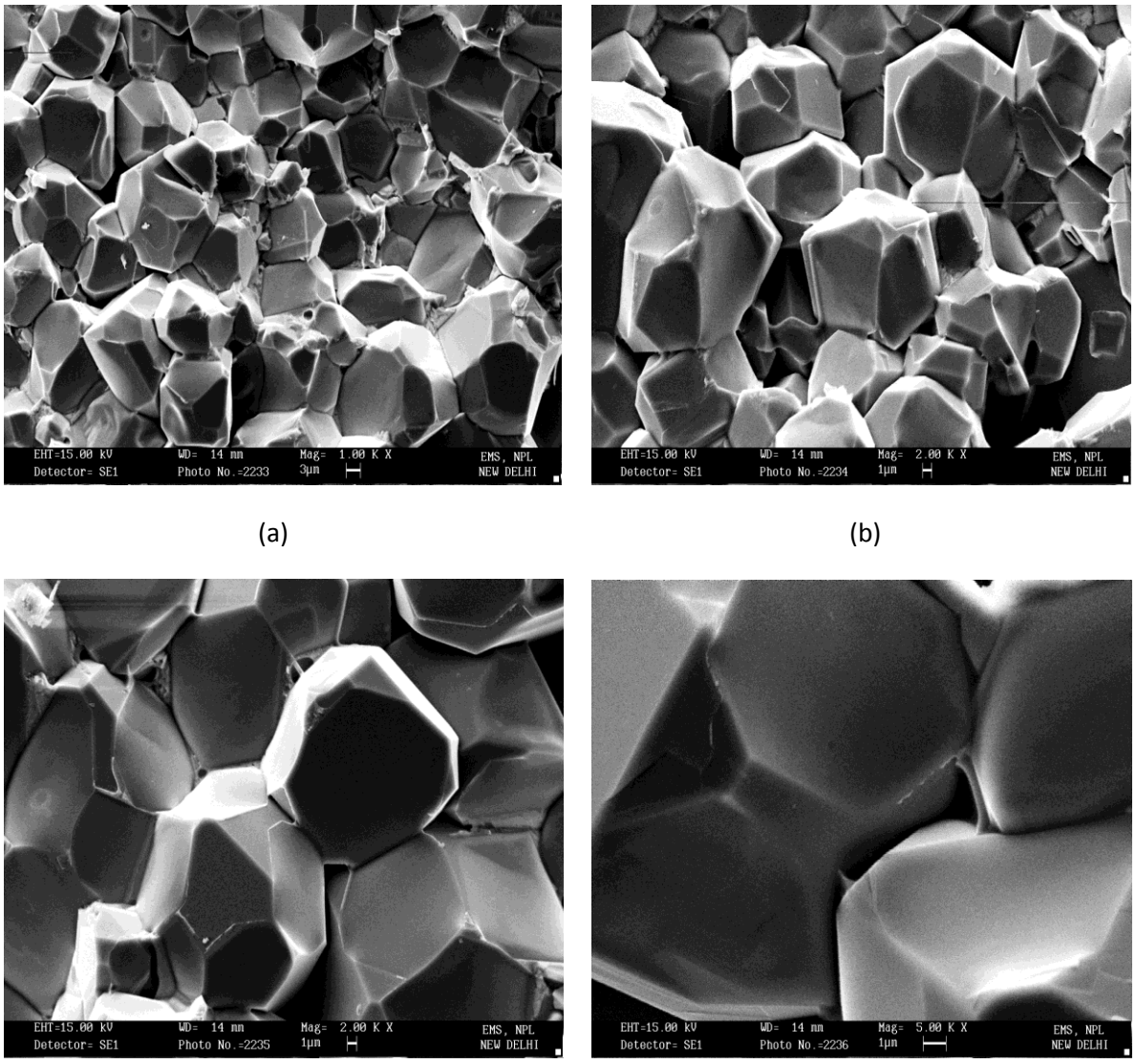

(a) (b)

(c) (d)

Fig. 5.4 SEM micrograph of CCTO sintered at 1050°C at different magnifications.

SEM micrograph of CCTO sintered at 1075°C for 10 h is shown in figure 5.5. The biggest grain is of 26 μm in diameter while smallest is of 17 μm in diameter. Porosity is more.

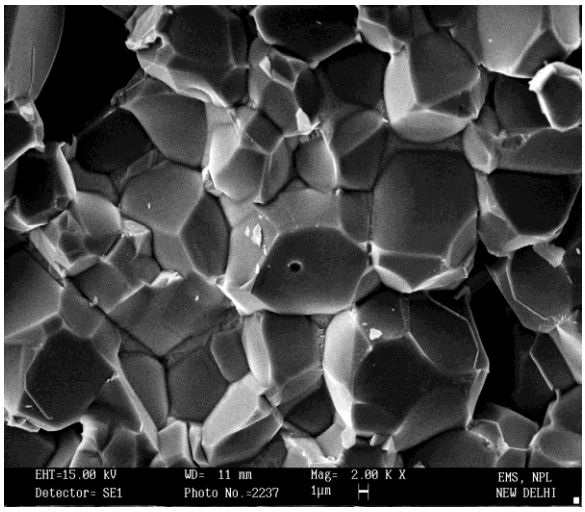

(a)

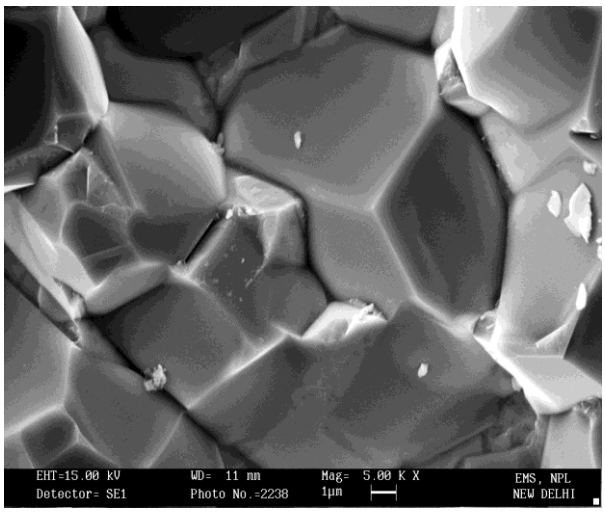

(b)

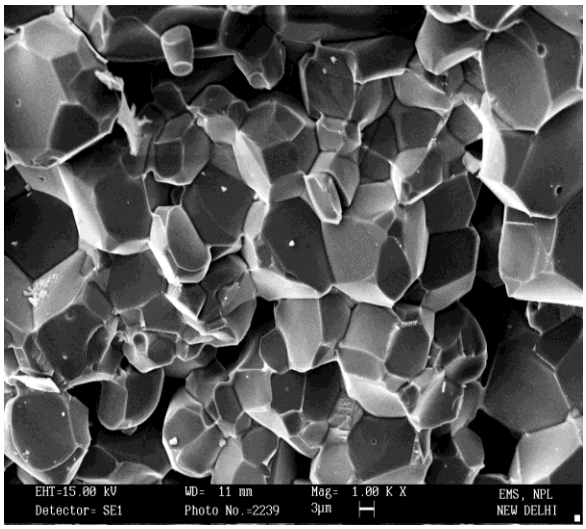

(c)

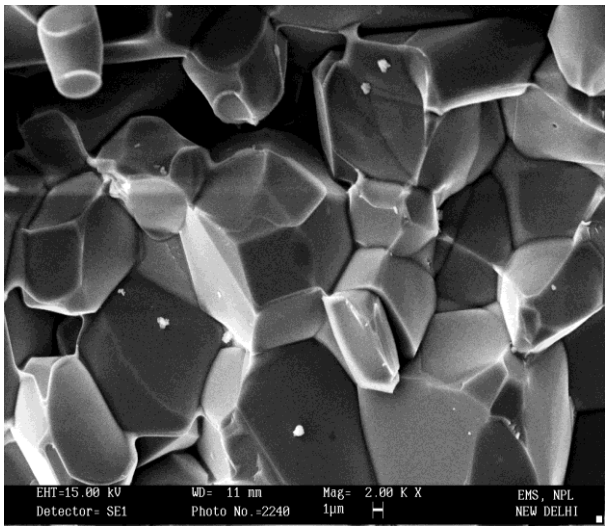

(d)

Fig. 5.5 SEM micrograph of CCTO at 1075°C at different magnifications.

SEM Micrograph of Calcium copper titanate sintered at 1100°C for 10 h is given in fig 5.7. The biggest grain is of 26 µm in diameter while smallest is of 17 µm in diameter. Porosity is more.

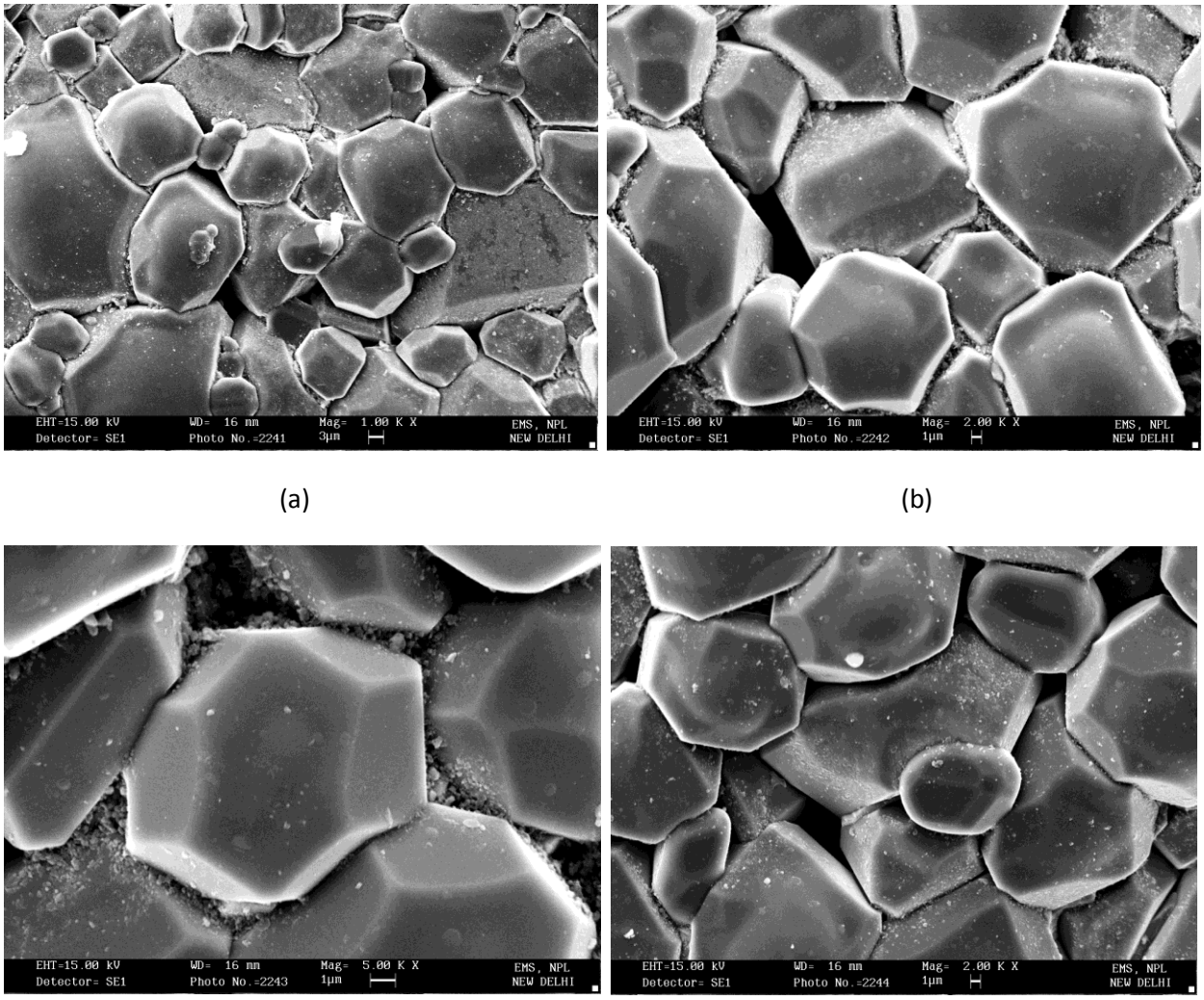

Fig. 5.6 SEM micrograph of CCTO at 1100°C at different magnifications.

SEM images of surface morphologies for the specimens sintered at different temperature for 10 h are shown in (figures 5.3-5.6). The morphologies change significantly with the sintering temperature. As the sintering temperature increases, the average grain size (d_G) was increased from 13 µm to 26 µm when temperature is increased form 1025°C to 1100°C for the same sintering time. Fracture grains are present at 1025°C but it is not present at higher temperature.

5.3 Analysis of dielectric properties:

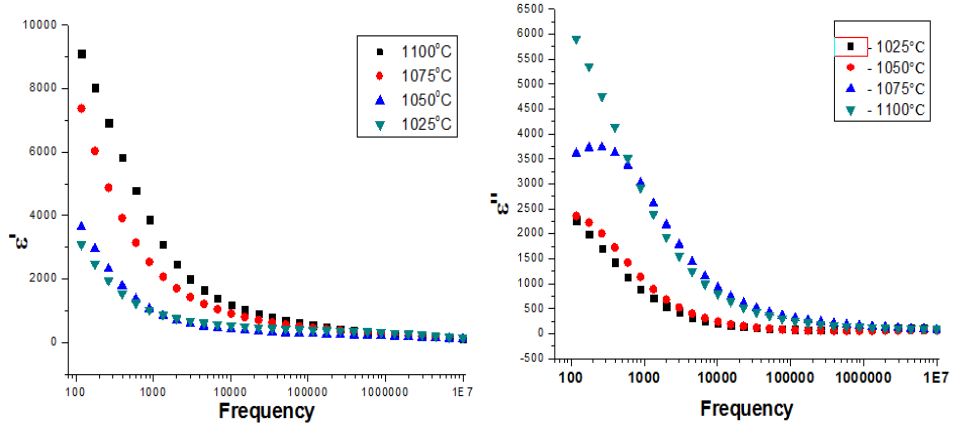

Fig. 5.7 Effect of permittivity on sintering temperature for 2 h.

The dielectric constant versus frequency for CCTO with different sintering temperature is plotted in figure 5.7. As seen in the plot, dielectric constant increased by increasing the sintering temperature at frequency up to 1000 Hz. Fig. 5.8 also confirms this result that the dielectric loss decreases with frequency at low frequencies but increases with frequency at high frequencies. Therefore, the reduction in dielectric loss of CCTO system can be attributed to the change of grain boundary resistance.

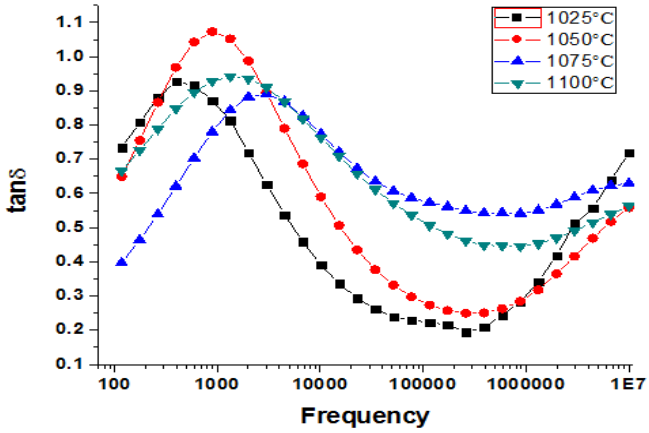

Fig. 5.8 Effect of tan delta on sintering temperature for 2 h.

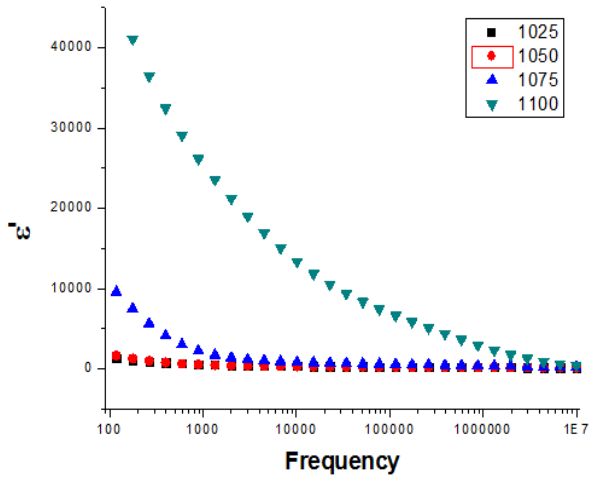

Fig 5.9 Effect of Real part of Dielectric constant on sintering temperature for 10 h.

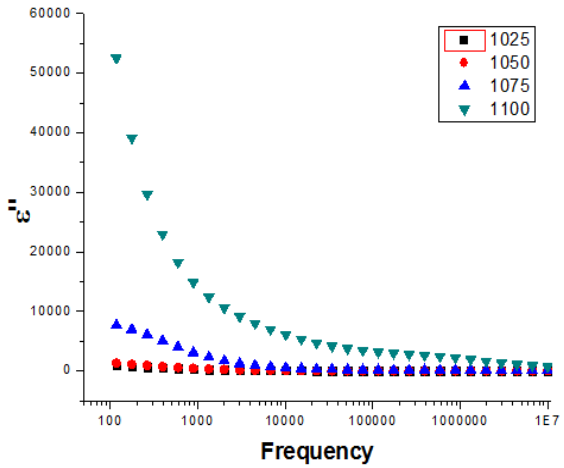

Fig 5.10 Effect of Imaginary part on Dielectric constant on sintering temperature for 10 h.

The increasing in dielectric constant may be correlated with porosity of the sample. The microstructural study revealed that the samples sintered at 1100°C/10 h have lower porosity than that sintered at 1100°C/2 h.

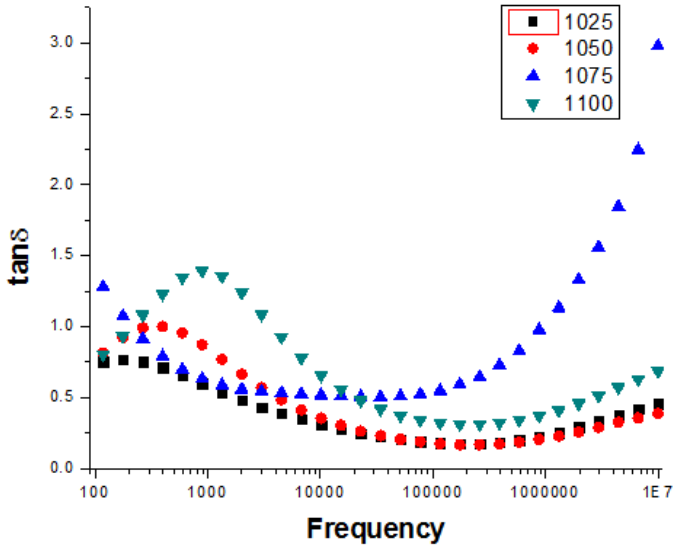

Fig. 5.11 Effect of tanδ on sintering temperature for 10 h.

The grain size of the samples sintered at 1100°C/10 h also high than that sintered at 1100°C/2 h. It could be found that the dielectric constant of the samples sintered at 1100°C for 10

h is higher than 10^4 at frequency range from 10^2 to 10^5 Hz. The giant permittivity value for ceramics is therefore associated with the presence of either thin reoxidized grain boundary regions on the outer surfaces of the large semiconducting grains or to a secondary phase at the grain boundaries [13] which has not been detected by XRD and SEM (Figs.5.2 and 5.6). Further work is needed to distinguish these possibilities. However in the present study the same could not be observed in the studied frequency range.

CHAPTER 6

CONCLUSIONS

CCTO is prepared by conventional solid state reaction method from ball milled powder. XRD results reveals peaks corresponding to cubic perovskite structure. The disordering in samples decreased with increasing heat treatment time. Moreover, XRD results show the formation of single phase. The SEM show formation of well defined grain. The grain sizes increases with increasing sintering temperature with higher porosity. Dielectric studies of ball milled samples reveals that the dielectric constant is increased with increase in sintering temperature as well as holding time. The holding time results in increase in dielectric constant but tanδ remains constant.

Future Scope:

The desired results can be obtained after optimising process parameter. Moreover, the doping effect of higher valence and lower valence cation for Ti^{4+} cation might be beneficial to obtain the better dielectric properties of the present system.

References:

1. M.A.Subramanian, L.Dong, B.A.Resiner, A.W. Sleight, J. Solid State Chem., 2000, 151, 323-325.
2. B. Bochu, M. N. Deschizeaux, J. C. Joubert, A. Collomb, J. Chenavas, M. Marezio, J. Solid State Chem., 1979, 29, 291.
3. G. Raynor Canham, T. Overton, Descriptive Inorganic Chemistry, W. H. Freeman and Company, 2003, Chapter 20, third edition.
4. M. A. Subramanian, D. Li, N. Duan, B. A. Reisner, A. W. Sleight, J. Solid State Chem, 2000, 151, 323.
5. J. Li, M. A. Subramanian, Chemical Materials, 2004, 33, 322.
6. A. P. Ramirez, M. A. Subramanian, M. Gardel, G. Blumberg, D. Li, T. Vogt, S. M. Shapiro, Solid State Commun., 2000, 115, 217.
7. Homes, T. Vogt, S. M. Shapiro, S. Wakimoto, A. P. Ramirez, Science, 2001, 293, 673.
8. L. He, J. B. Neaton, M. H. Cohen, D. Vanderbilt, Phys. Rev. B, 2002, 65, 214-112.
9. A. J. Moulson, J. M. Herbert, Electroceramics, John Wiley & Sons Ltd., West Sussex, 2003, Chapter 5, second edition.
10. D. C. Sinclair, T. B. Adams, F. D. Morrison, A. R. West, Appl. Phys. Lett., 2002, 80, 2153.
11. J. T. S. Irvine, D. C. Sinclair, A. R. West, Adv. Mater., 1990, 2, 132.
12. J. K. Beddow, Particulate Science and Technology; Chemical Publishing Co.: New York, 1980.
13. A. J.Moulson, J. M. Herbert, Electroceramics, John Wiley & Sons Ltd., West Sussex, 2003, Chapter 5, second edition.

14. M.N.Rahaman, Ceramic Processing and Sintering. 2nd Edition.
15. “Sintering furnace”. http://www.crystec.com/kllsinte.htm.
16. J. Daintith, “Biographical Encyclopedia of Scientists” CRC Press, 1994, 943.
17. F. Rossignol , A. Rumeaud, T. Lebey , E. Dutarde B. Barbier, C. Combettes , S. Guillemet Fritsch , T. Chartier ,2009, 29, 731-735.
18. Jianjun Liu, Robert W. Smith, Wai Ning Mei, Chem. Mater. , 2007, 19, 6020-6024.
19. Jianjun Liu, Yucheng Sui, Chun gang Duan, Wai Ning Mei, Robert W. Smith, John R. Hardy, Chem. Mater., 2006, 18, 3878-3882.
20. Shuhua Jin , Haiping Xia, Yuepin Zhang , Juping Guo , Jun Xu, Materials Letters, 2007, 61, 1404-1407.
21. Kang Min Kim, Sun Jung Kim, Jong Heun Lee, Doh Yeon Kim, Journal of the European Ceramic Society, 2007, 27, 3991-3995.
22. C.C. Wang, Y.J. Yan, L.W. Zhang, M.Y. Cui, G.L. Xie, B.S. Cao, Scripta Materialia, 2006, 54, 1501-1504.
23. Ben Peng Zhua, ZiYu Wanga, Yue Zhanga, ZhiSong Yua,b, Jing Shia,c, Rui Xiong, Materials Chemistry and Physics, 2009, 113, 746-748.
24. Sabar D. Hutagalung , M. Ikhwan M. Ibrahim, Zainal A. Ahmad, Ceramics International, 2008, 34, 939-942.
25. P.Thomas , K.Dwarakanath , K.B.R. Varma , T.R.N. Kutty, Journal of Physics and Chemistry of Solids, 2008, 69, 2594-2604.
26. Y.J. Kim, S.Wakimoto, S.M. Shapiro, P.M. Gehring, A.P. Ramirez, Solid State Communications, 2002, 121, 625-629.

27. Chivalrat Masingboon, Prasit Thongbai, Santi Maensiri , Teerapon Yamwong, Supapan Seraphin, Materials Chemistry and Physics, 2008, 109, 262-270.
28. P. Jha, P. Arora, A.K. Ganguli, Materials Letters, 2003, 57, 2443-2446.
29. AndrewE.Smith, T.G.Calvarese, A.W.Sleight, M.A.Subramanian, Journal of Solid State Chemistry, 2009, 182, 409-411.
30. Laijun Liu, Huiqing Fan, Pinyang Fang, Li Jin, Solid State Communications , 2007, 142, 573-576.
31. M.A. Subramanian, W.J. Marshall, T.G. Calvarese, A.W. Sleight, Journal of Physics and Chemistry of Solids, 2003, 64, 1569-1571.
32. G. Chiodelli,, V. Massarotti, D. Capsoni, M. Bini, C.B. Azzoni, M.C. Mozzatic, P. Lupotto, Solid State Communications, 2004, 132, 241-246.
33. Yu Hongtao, Liu Hanxing, Dabing Luo, Minghe Cao, journal of materials processing technology, 2008, 208, 145-148.
34. Sabar D. Hutagalung, M. Ikhwan M. Ibrahim, Zainal A. Ahmad, Ceramics International, 2008, 34, 939-942.
35. Sabar D. Hutagalung, Mohd Ikhwan M. Ibrahim, Zainal A. Ahmad, Materials Chemistry and Physics, 2008, 112, 83-87.
36. Alexander Tselev, Charles M. Brooks, Steven M. Anlage, Physical Review 70, 2004, 144-181.
37. S. F. Shao, J. L. Zhang, P. Zheng, W. L. Zhong, C. L. Wang, J. Applied Physics, 2006, 99, 84-106.
38. F.Kremer, A.Schonhals, Luck W. Broadband Dielectric Spectroscopy. Springer Verlag, 2002.

39. A. M.Sidorovich, Dielectric Spectrum of Water. Ukrainian Physical Journal, 1984, 29, 1175-1181.
40. A. R.Hippel, Dielectrics and Waves. N. Y.: John Willey & Sons, 1954.
41. A.A.Volkov, A.S.Prokhorov, Broadband Dielectric Spectroscopy of Solids. Radiophysics and Quantum Electronics, 2003, 46, 657-665.